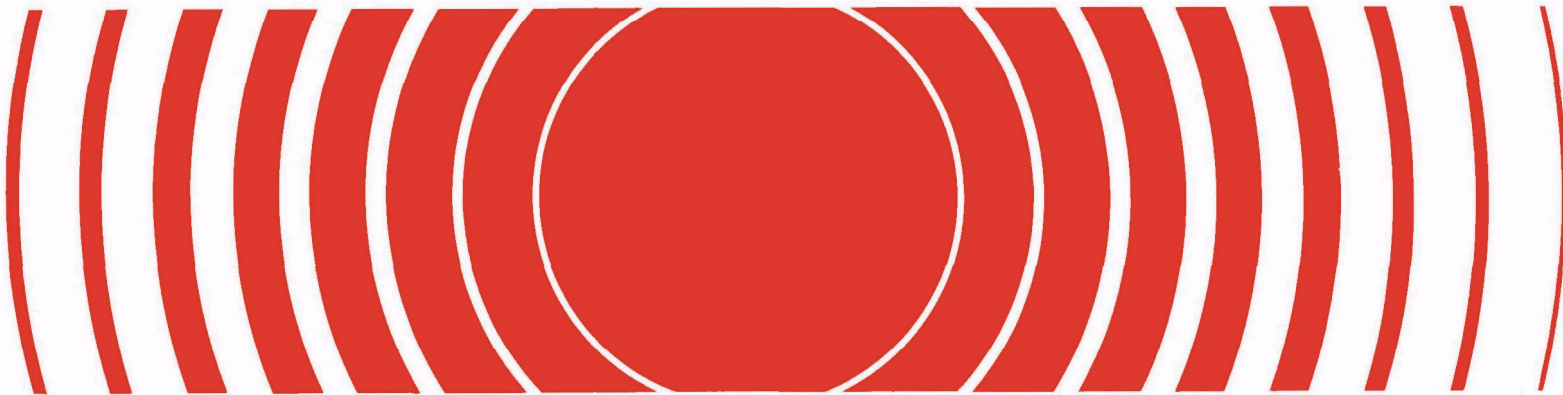




Ocean Current Measurements At The Farallon Islands Low-Level Radioactive Waste Disposal Site 1977 - 1978



Ocean Current Measurements
at the
Farallon Islands
Low-Level Radioactive Waste Disposal Site
1977 - 1978

Prepared under
Contract 68-01-0796

Project Officer
Robert S. Dyer
Office of Radiation Programs
U.S. Environmental Protection Agency
Washington, D.C.



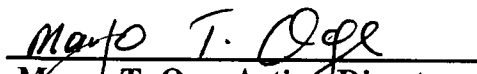
FOREWORD

Pursuant to Public Law 92-532 (the Marine Protection, Research and Sanctuaries Act of 1972), the U.S. Environmental Protection Agency (EPA) has developed criteria and regulations to govern ocean disposal of all forms of waste, including low-level radioactive waste (LLW) materials.

In 1974, the EPA Office of Radiation Programs (ORP) initiated feasibility studies to determine whether existing technologies could be applied toward assessing the fate of radioactive wastes that had previously been disposed in the oceans. The ORP developed a program for site characterization studies to determine the biological, chemical, geological and physical characteristics of the marine environment in and near sites that had been designated by the former Atomic Energy Commission (AEC) for ocean disposal of LLW. These studies also included investigating the presence and distribution of radionuclides within these sites.

A primary mechanism for physically dispersing and redistributing both soluble and particulate radioactive materials from a disposal site is the action of ocean bottom currents. Of particular interest is the magnitude and direction of these currents. This report discusses the results of ocean bottom current measurements obtained from the Farallon Islands LLW disposal site off the California coast, near San Francisco. The report includes a discussion of the velocity of the currents over the time period and area measured relative to large-scale currents off the California coast, and the possibility for shoreward transport of LLW materials from the Farallon Islands site.

The Agency invites all readers of this report to send any comments or suggestions to Mr. Martin P. Halper, Director, Analysis and Support Division, Office of Radiation Programs (ANR-461), U.S. Environmental Protection Agency, Washington, DC 20460.


Margo T. Oge, Acting Director
Office of Radiation Programs

CONTENTS		
<u>Section</u>		<u>Page</u>
1.	INTRODUCTION	1
2.	SUMMARY	3
2.1	DESCRIPTION OF STUDY	3
2.2	RESULTS AND CONCLUSIONS	3
3.	MEASUREMENT PROGRAM	7
3.1	OPERATION AND OBJECTIVES	7
3.2	DESCRIPTION OF HARDWARE	8
3.3	CURRENT METER ARRAY LOCATION AND OPERATION	9
3.4	BATHYMETRY	15
3.5	SEDIMENT INFORMATION	15
4.	DATA REDUCTION	18
4.1	CURRENT METER DATA	18
4.2	GENERATION OF BATHYMETRIC CHART	18
4.3	GRAIN SIZE FROM SEDIMENT SAMPLES	19
5.	CURRENT METER DATA PROCESSING	21
5.1	DATA PRODUCTS	21
5.2	VACM AND AANDERAA COMPARISON	35
5.3	MEASUREMENT ACCURACY AND TIMING ERRORS	41
5.4	CONDUCTIVITY AND SALINITY	45
6.	DATA INTERPRETATION	46
6.1	ANALYSIS OF CURRENTS	46
6.2	TRANSPORT POTENTIAL	62
7.	RECOMMENDATIONS FOR FURTHER WORK	68
8.	REFERENCES	71
APPENDICES [Contained In A Separate Report - EPA 520/1-91-009/A]		
	TIME HISTORY - SPEED AND DIRECTION	A-1
	TIME HISTORY PLOTS - NORTH, EAST CURRENTS	B-1
	HISTOGRAMS	C-1
	SCATTERGRAMS	D-1
	SPECTRA - NORTH, EAST COMPONENTS	E-1
	PROGRESSIVE VECTOR DIAGRAMS	F-1
	STICK PLOTS	G-1
	SUMMARY STATISTICS	H-1

LIST OF FIGURES

<u>Number</u>		<u>Page</u>
1-1	Locator Chart	2
2-1	Current Meter Arrays for Radioactive Waste Disposal Site	4
3-1	Current Meter Locations	11
3-2	Data Coverage Plot 1977-1978	12
3-3	Profile Schematic	13
3-4	Current Meter Array Plan Schematic	14
3-5	Locations of Core Sample Sites	16
3-6	Depth Profile of Core Sample Sites	17
4-1	Bathymetry Chart	20
5-1	Time History Plot, Current Speed, and Direction (Meter 2920)	22
5-2	Time History Plot, North Current, East Current (Meter 2920)	24
5-3	Histogram Current Speed (Meter 2920)	26
5-4	Speed Versus Direction Scattergram (Meter 2920)	28
5-5	Power Spectrum (Meter 2920; February 1978)	29
5-6	Progressive Vector Diagram (Meter 2919)	31
5-7	Stick Plot (Meter 2918)	33
5-8	Summary Statistics (Meter 2919)	34
5-9	VACM Reconstruction 1	37
5-10	VACM Reconstruction 2	38
5-11	VACM Reconstruction 3	39
5-12	VACM Reconstruction 4	40
5-13	Speed Gain Transfer Function for Meter 2830 Versus VACM	42
5-14	Speed Phase Transfer Function for Meter 2830 Versus VACM	43
6-1	Power Spectrum for Meter 2918	50
6-2	Power Spectrum for Meter 2919	51
6-3	Power Spectrum for Meter 2830	52
6-4	Power Spectrum for VACM	53
6-5	Power Spectrum for Meter 2920	54
6-6	Tidal Ellipse Calculation	55
6-7	Tidal Ellipse for Meter 2918	56
6-8	Tidal Ellipse for Meter 2919	57
6-9	Tidal Ellipse for Meter 2830	58
6-10	Tidal Ellipse for VACM	59
6-11	Tidal Ellipse for Meter 2920	60
6-12	Exceedence Curves for Total Measurement Periods	66
6-13	Exceedence Curves for October through December 1977	67

LIST OF TABLES

<u>Number</u>		<u>Page</u>
3-1	Farallon Islands Current Meter Locations	9
3-2	Data Record	10
3-3	Box Cores Collected for Sediment Studies During R/V VELERO IV Cruise (August-September 1977)	15
5-1	Estimated Clock Drift	44
6-1	Major Current Energy Sources for Entire Operating Period of Each Meter	49
6-2	Vector-averaged Current Velocities	61
6-3	Sediment Surface Grain Size Data from Farallon Islands LLW Site Survey Cores	63
6-4	Percent of Total Time Measurement Speeds Exceed 20 cm/s	65

1. INTRODUCTION

This report describes the work performed by Interstate Electronics Corporation (IEC) under contract to the U.S. Environmental Protection Agency's (EPA) Office of Radiation Programs (ORP). It presents data from an ocean current measurement study, conducted during 1977 and 1978, in the area of the U.S. low-level radioactive waste (LLW) disposal site near the Farallon Islands (Figure 1-1) off the coast of San Francisco, California. It also contains other oceanographic and environmental data acquired from the same area.

The purpose of this study was to measure near-bottom and bottom currents in the area, and utilize available historical data, to determine the potential for transport of LLW from the disposal site toward populated areas in the vicinity of San Francisco. The remainder of this report is sub-divided into sections, as follows:

Section 2 describes the study and summarizes results and conclusions;

Section 3 discusses the measurement program that generated the data analyzed in this report;

Section 4 describes the steps taken to improve the quality of data from two of the current meters, and gives an assessment of the overall quality and temporal coverage of the current meter data;

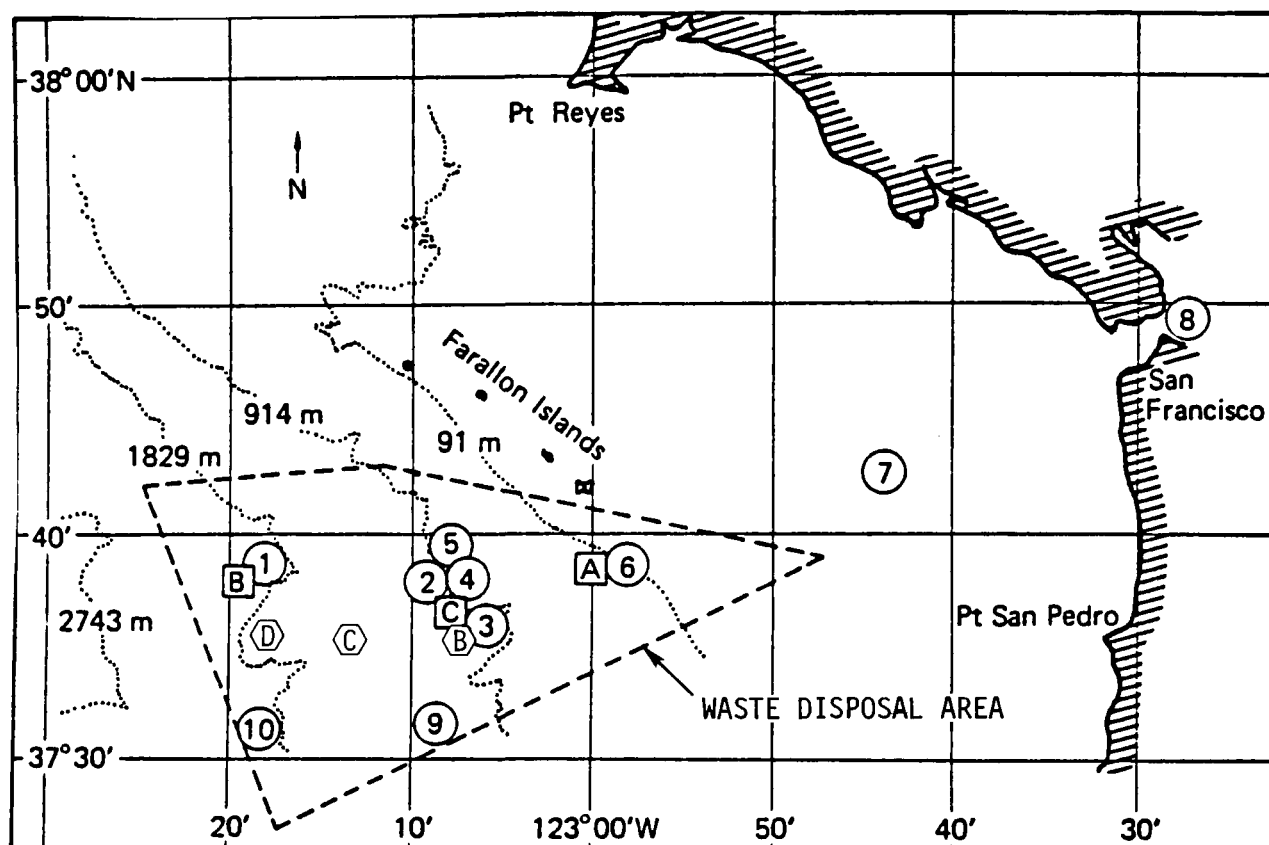
Section 5 discusses data processing and verification;

Section 6 contains an interpretation of the current meter data combined with other available data taken at the site during previous studies conducted in 1974 and 1975, including an analysis of the current, sediment, and bathymetric data and of transport mechanisms related to the data;

Section 7 contains recommendations for future sampling;

Section 8 lists the references utilized during the study; and,

the Appendices contain computer generated graphical displays of the current meters' output data.



- DUMP SITES
- STATIONS SAMPLED FOR WATER, SEDIMENT, OR BIOTA
- ⬡ CURRENT METER ARRAYS

Figure 1-1. Locator Chart.

Dashed line indicates area defined ^[1] as the Waste Disposal Area; squares A, B, and C are disposal sites. Circled numbers 1 through 10 are the locations of January 1977 sampling stations ^[2]. Hexagons B, C, and D indicate the locations of current meter arrays during this (1977-1978) study.

2. SUMMARY

This section briefly summarizes the major events of this current measurement program, the subsequent analysis of data, and the conclusions obtained. The analysis of data included the following five tasks: (1) assessing data quality, (2) comparing data from the different types of current meters used, (3) determining relative clock drift and timing errors, (4) evaluating the measured current components, and (5) estimating potential for sediment transport of LLW from the disposal site. The conclusions derived from each task are given in Sub-Section 2.2., below. Examples to support these conclusions are discussed in the appropriate portions of Sections 3 through 7 of this report.

2.1 DESCRIPTION OF STUDY

In October 1977 four mooring line arrays containing seven current meters were deployed in the vicinity of the LLW disposal site near the Farallon Islands (Figure 2-1). The instruments on the arrays included six Aanderaa model 5 Recording Current Meters (RCM), and one Sea-Link Vector-Averaging Current Meter (VACM). All were pre-set for an operational period of approximately 90 days, but actual deployment lasted for about a year.

During recovery, in October 1978, it was observed that many of the meters were capable of continuous data recording for a longer period of time than was expected (Figure 3-2). This is especially true for the VACM, which continued to record data for the entire year.

It was also observed during recovery that the transmitter on the acoustic release mechanism for Array A did not transmit when interrogated. When the release mechanism was activated the array could not be located. Thus, two of the RCM 5 meters (numbers 2916 and 2917) were lost.

2.2 RESULTS AND CONCLUSIONS

2.2.1 Data Quality

Data was recovered from five current meters--four Aanderaas and one VACM. The VACM recorded data for 1 year, while the Aanderaas recorded for a period of 2 to 4½ months each. After recovery of the meters and subsequent initial inspection, it was observed that the VACM was still recording data, while two of the Aanderaa meters (numbers 2919 and 2920) had filled their output tapes. The other two Aanderaa meters (numbers 2830 and 2918) had experienced battery failures during their operation. Details regarding the operation and performance of the hardware can be found in Sections 3.1 and 3.3.

All of the data recovered from the VACM and two of the Aanderaa meters (numbers 2918 and 2919) was of a quality suitable for analysis and interpretation. The data from the other two Aanderaa meters (numbers 2830 and 2920) had to be recovered by a special technique, as described in Section 4.1, but after this additional processing it was also found to be of good quality. There were a few isolated data points in some of the records for each of the meters which had obvious nonphysical values due to either electronic noise or mechanical problems, but these were replaced by interpolated values yielding a continuous record of high quality. The data was then translated to metric engineering units for analyses and generation of data products. See Section 4.1 for further discussion.

The statistical properties of the recovered data were generally in accordance with expected physical processes, although it became evident that the VACM data record contained a number of transpositions in data sequence. In addition, Aanderaa # 2830 apparently contained gaps in its recording. Approximately 9 hours of data were missing from the beginning of the record commencing October 26, 1977. Further discussion appears in Section 5.2.

2.2.2 Comparison of the VACM and Aanderaa Meters

After taking into account the observed inconsistencies in the VACM data sequence, the corresponding VACM and Aanderaa meter # 2830 records were compared by examining the time series and obtaining the speed transfer function. The data records were found to be a relatively close match. The speed transfer function was relatively flat and fell within a range of 0.8 to 1.05, with the VACM giving a generally larger magnitude than observed on meter # 2830. The phase portion of the transfer function was linear, indicating no substantial timing rate shifts between the two meters (see Section 5.2).

2.2.3 Relative Clock Drift

The semidiurnal tidal occurrences were examined to determine the degree of relative clock drift for the 5 meters. Analyses in both the time and frequency domains indicated that although clock drift appeared to be of a larger magnitude than advertised by the meter manufacturers, relative timing errors were within a range suitable for cross-analysis of all five current meter data records. Section 5.3 addresses the details of this analysis.

2.2.4 Evaluation of Measured Current Components

For each meter the short-term periodic and long-term average current components were examined (see Section 6.1) with the following results:

- a. In the deep western part of the dump site, most of the current energy is from 12-hour tides in the east-west direction;

- b. In the deep eastern part of the dump site, most of the current energy is from 12-hour tides with a slightly greater component of energy in the north-south direction;
- c. The total current energy is significantly greater in the deep western portion of the site than in the deep eastern portion;
- d. The VACM and Aanderaa meter # 2830 in the open ocean (midwater) show a relatively equal distribution of tidal energy and also have a significant low frequency component in the north-south direction; and,
- e. Long-term currents average less than 2 cm/s and move in the northeast direction for the bottom measurements (Aanderaa meters 2918, 2919, and 2920) and the southeast direction for the deep midwater (VACM and Aanderaa # 2830) measurements.

2.2.5 Estimation of Sediment Transport Potential

Analysis of sediment distributions has indicated that fine-grain sediments composed the majority of sediment volume [3]. Since these sediments can occasionally be suspended when water velocities exceed about 20 cm/s, an estimate of transport potential was obtained by determining the extent to which these velocities occur. Average currents were then used to determine the probable distance and direction of transport (see Section 6.2). The general conclusions are as follows:

- a. In the deep western part of the site, current measurements exceed 20 cm/s no more than 3 percent of the time. This may be sufficient to suspend fine-grain sediments (silt and clay), providing a potential for transport in the water column.
- b. Long-term average near-bottom currents move north and eastward throughout the site. Average current speeds diminish from 1.7 cm/s at the deep western end of the site to 0.17 cm/s at the eastern end, thus it appears that this vector decreases with proximity to the shore.
- c. Results, though inconclusive, indicate that there may be reason to further investigate the extent and scale of transport as it relates to contaminated sediment.

3. MEASUREMENT PROGRAM

On October 25, 1977 four arrays containing six Aanderaa current meters and one VACM were installed in an area of the radioactive waste disposal site near the Farallon Islands (Figure 1-1). This section discusses the procedures and operations used in the deployment of the meters and the subsequent acquisition of data.

3.1 OPERATION AND OBJECTIVES

A total of seven current meters were to be emplaced using four arrays, supported by subsurface buoys (Figure 2-1). One array (A) was lost, consequently no data were recovered from Aanderaa meters 2916 and 2917. The remaining four Aanderaa meters and the VACM functioned and recorded current velocity, temperature, and conductivity measurements for between 2 months and 1 year for each meter, giving a cumulative volume of data totaling 800 days.

The selection of the current measurement hardware was based on a number of factors including (1) cost, (2) anticipated performance at the depths and durations required for this program, and (3) known handling and reliability characteristics. The Aanderaa RCM, model 5, was deemed most suitable in terms of these considerations. The VACM was deployed immediately above one of the Aanderaa meters in order to study the operational characteristics of the two meter types relative to each other.

The study was designed to provide preliminary information about the speed and direction of water moving through the region of the disposal site. This information, along with the results of previous physical and chemical studies of the region, was intended to aid in the development of an understanding of the natural physical processes and any subsequent impact related to potential or existing transport of radioactive materials from the disposal area.

Deployment of the arrays (Figure 2-1) was planned to establish two approximately triangular planar surfaces of measurement; one parallel to and within a few meters of the bottom, (arrays A, B, and D, and the other approximately parallel to the 3,000-foot depth level (arrays A, B, and C). In addition, the positioning the VACM and Aanderaa meter # 2830 close together on the same string would allow for a direct comparison of these two meter types in a midwater location, where the assumption could be made that both meters were experiencing the same water mass dynamics.

3.2 DESCRIPTION OF HARDWARE

The Sea-Link VACM records current speed and direction in cartesian coordinates, average water temperatures, and timing information sampled at an adjustable interval for a period as long as 1 year. Current speed is obtained from a savonius rotor, and direction is measured relative to magnetic north by means of a neutrally buoyant magnetic-coupled vane mounted above the rotor.

The VACM records eight current speed and direction measurements with each turn of the rotor. The readings are divided into components, combined, and referenced to time and temperature on a cassette tape recorder at preselected intervals. This averaging is believed to filter out high frequencies caused by mooring motion. A 15-minute interval was selected for this measurement program. The meter is powered by a self-contained alkaline battery pack with a life expectancy of 9 months at an average current speed of 150 cm/s. The operational ranges and accuracies for measured parameters are:

Current speed:	2.5 to 300 cm/s
Current direction:	0° to 360° ±2.8°
Temperature:	-2°C to 35°C ±0.10°C
Timing accuracy:	6 minutes/year

The Aanderaa RCM-5 current meter also uses a savonius rotor to record current speed. The meter is mounted in front of a large vane so that the rotor is always pivoted into the oncoming current. In addition to current speed and direction and water temperature, the instrument may contain optional devices for measuring conductivity and water depth. One of the meters used in this study, # 2920, recorded conductivity by means of an inductively coupled toroidal coil. The measurement interval was preselected at 20 minutes to allow for approximately 4 months of recording. Battery life is 3 months. Operational ranges and accuracies for measured parameters are:

Current speed:	1.5 to 250 cm/s
Current direction:	0° to 360° ±0.1°
Conductivity:	0.0 to 60 millimho/cm
Timing accuracy:	12 minutes/year

Aanderaa RCM's have demonstrated compass errors due to magnetization of nickel plating in pressure cases. The meters deployed for this survey used new epoxy-coated pressure cases with nickel only in the upper 0-ring region.

3.3 CURRENT METER ARRAY LOCATION AND OPERATION

Table 3-1 and Figure 3-1 give the locations, site depths, and meter depths of each current meter in the water column. Figure 3-1 also shows the local bathymetry in relation to the current meters. The meters were deployed along a gully running roughly east-west. The VACM and Aanderaa meter # 2830 were attached on the same array anchored at the bottom in a depression, and the other Aanderaa meters were anchored on a ridge just north of the gully with meters 2918 and 2919 attached on the same array. Bottom topography increased from east to west.

Table 3-1. Farallon Islands Current Meter Locations

Meter (Array)	Start	End	North Latitude	West Longitude	Site Depth (m)	Meter Depth (m)
Aanderaa 2920 (B)	10/25/77	3/15/78	37°36'36"	123°07'32"	914	911
Aanderaa 2830 (C)	10/25/77	2/06/78	37°36'52"	123°14'46"	1372	912
VACM (C)	10/25/77	10/24/78	37°36'52"	123°14'46"	1372	911
Aanderaa 2918 (D)	10/25/77	12/21/77	37°36'51"	123°17'27"	1829	1800
Aanderaa 2919 (D)	10/25/77	3/10/78	37°36'51"	123°17'27"	1829	1826

Table 3-2 and Figure 3-2 show the beginning and end of the data records, and the number of days of recorded data for each current meter. The four Aanderaa meters recorded from 57 to 141 days of data at 20-minute intervals while the VACM recorded one complete year of data at 15-minute intervals.

Figures 3-3 and 3-4 show the meter array schematically in profile and plan views, respectively. The loss of the two meters on Array A (Figure 2-1) resulted in a loss of a third reference point, which was necessary for the full definition of the two planes discussed in Section 3-1; however, a sufficient amount of information was recorded by the remaining meters from which to draw preliminary conclusions.

Table 3-2. Data Record

Meter	Start Date	End Date	Number of Days	Number of Data Records
Aanderaa 2920	10/25/77	03/15/78	141	10154
Aanderaa 2830	10/25/77	02/06/78	104	7547
VACM	10/25/77	10/24/78	365	35018
Aanderaa 2918	10/25/77	12/21/77	57	4016
Aanderaa 2919	10/25/77	03/10/78	136	9800

Although the array was designed to acquire water flow information for 3 months, considerably more data were acquired, most notably from the VACM. The following observations were made during the recovery operation conducted on October 24, 1978, 1 year after deployment:

Meter # 2830 collected data on approximately 75 percent of the output tape before battery failure occurred. Timing problems with the tape drive mechanism necessitated a special data recovery technique described in Section 4.1.

Meter # 2918 collected data on about 50 percent of the tape before experiencing a battery failure.

Meters 2919 and 2920 had both completely filled their respective output tapes. Meter # 2920 had experienced tape drive problems similar to the problems experienced with meter # 2830 (see Section 4.1).

The VACM meter was still functioning at the time of its recovery.

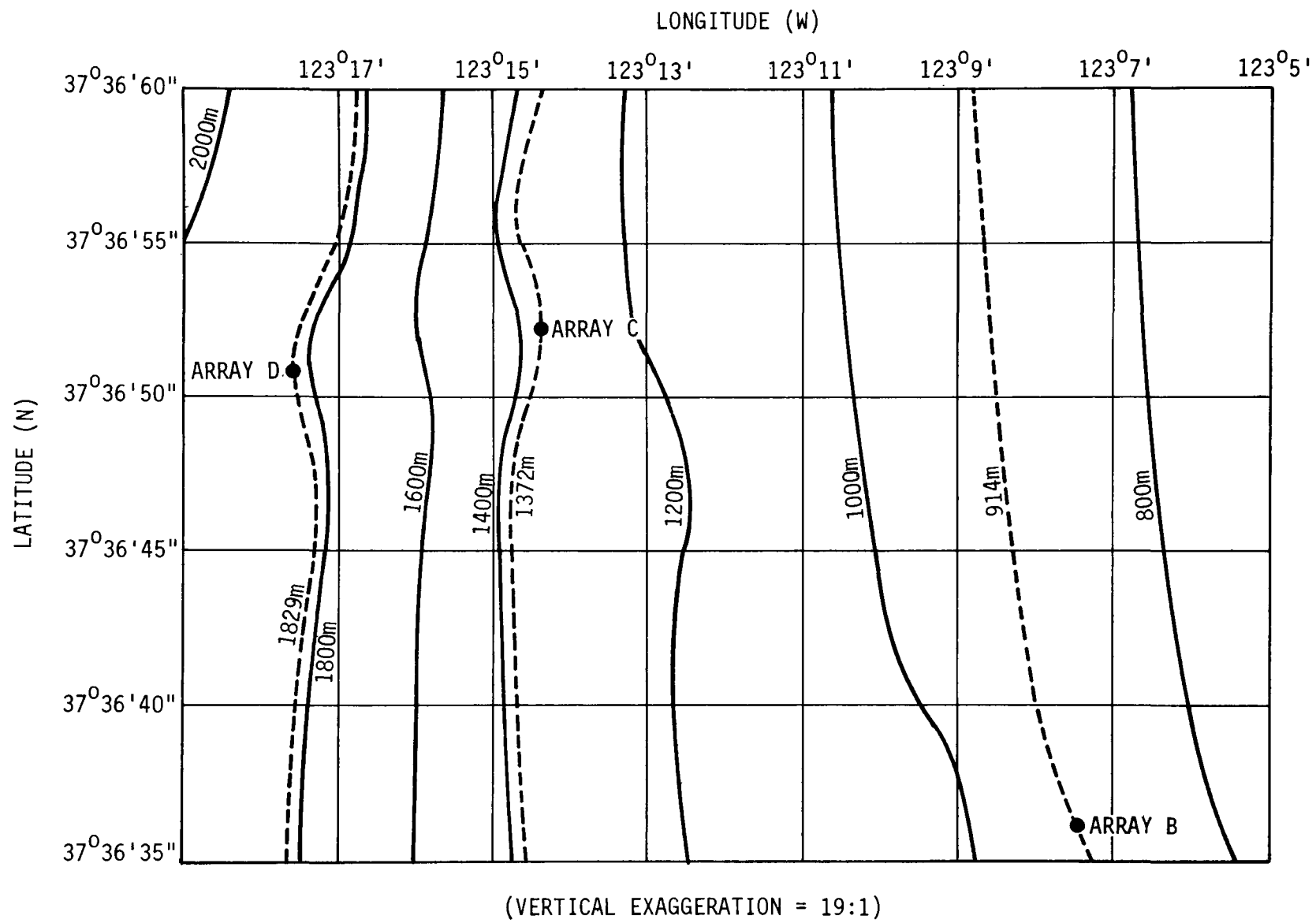


Figure 3-1. Current Meter Locations

AANDERAA
NO. 2918

57 DAYS

AANDERAA
NO. 2919

136 DAYS

AANDERAA
NO. 2920

141 DAYS

AANDERAA
NO. 2830

104 DAYS

VACM 365 DAYS

OCT	NOV	DEC	JAN	FEB	MAR	APR	MAY	JUN	JUL	AUG	SEP	OCT
1977			1978									

Figure 3-2. Data Coverage Plot 1977-1978

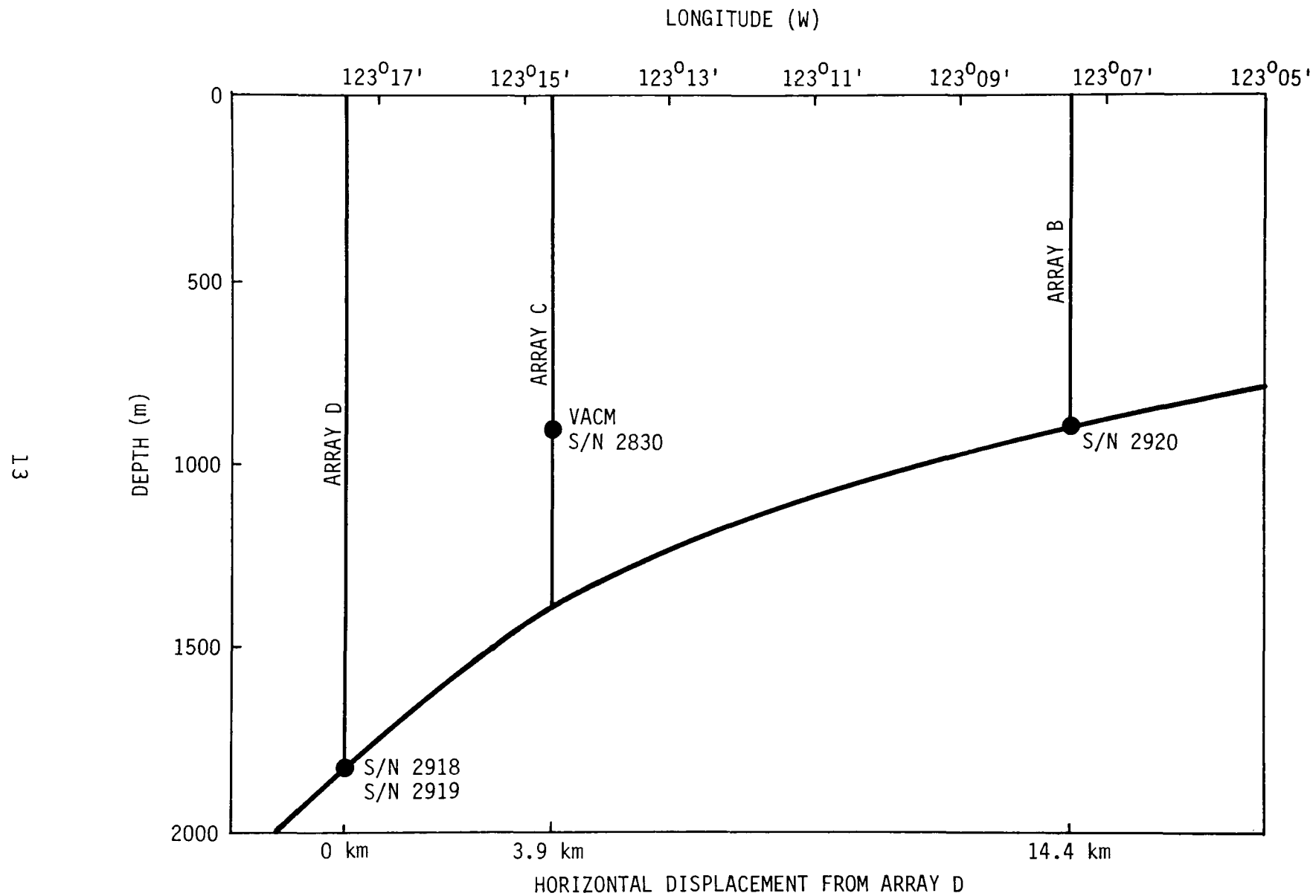
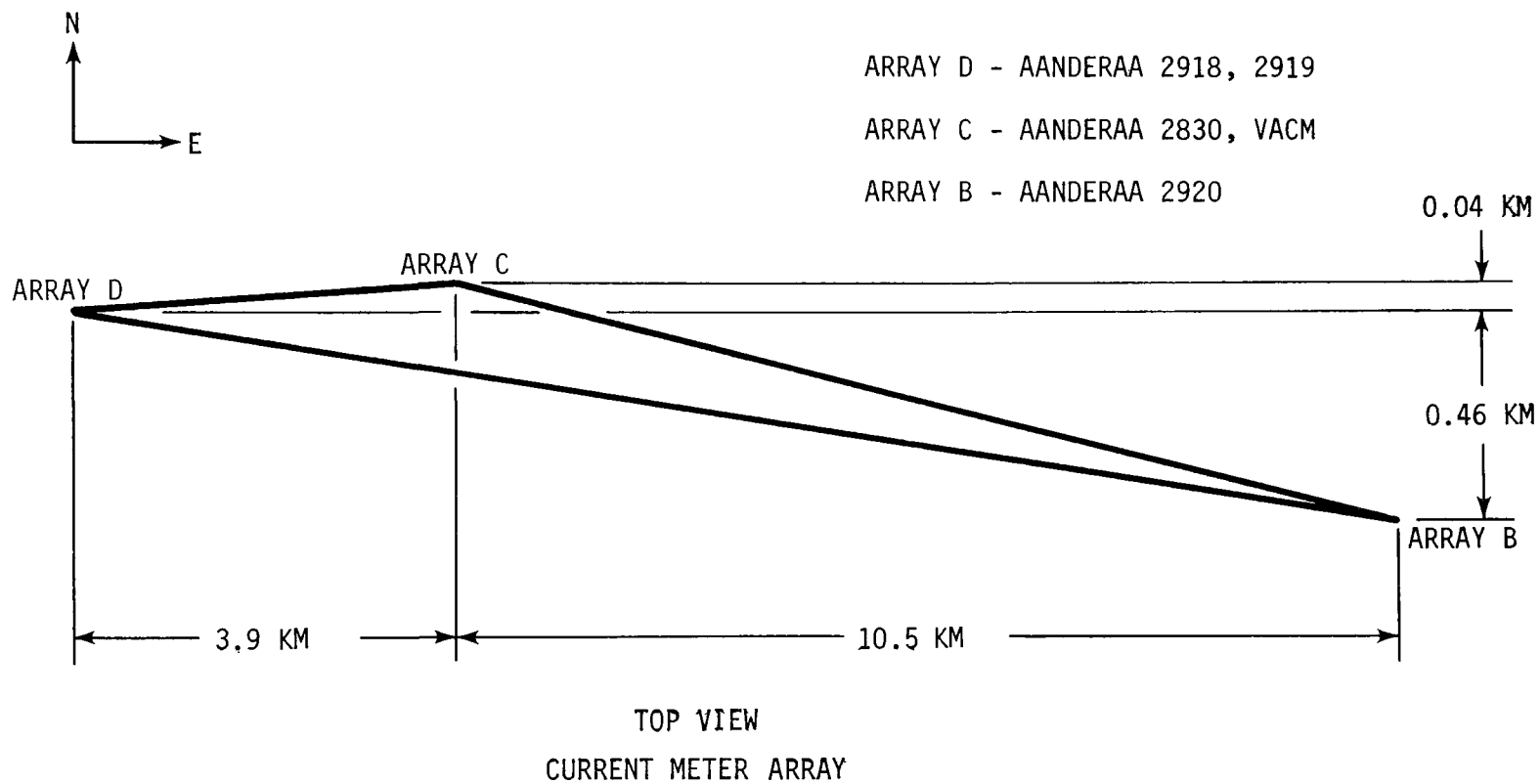


Figure 3-3. Profile Schematic



(HORIZONTAL SCALE = 10 TIMES VERTICAL SCALE)

Figure 3-4. Current Meter Array Plan Schematic

3.4 BATHYMETRY

Bottom depth profiles were acquired during surveys of the Farallon Islands LLW disposal site in 1974, 1975, and 1977. The equipment used during the 1977 survey consisted of two precision depth recorders, a GIFFT recorder serving as the primary sounding device, and an EDO-Western recorder for backup. Sounding profiles were made with both devices.

Navigation equipment for the 1977 survey included a Motorola Mini-Ranger III, which received reference signals from Point Reyes and Montara Point. This allowed position readings with an estimated accuracy of approximately 200 meters.

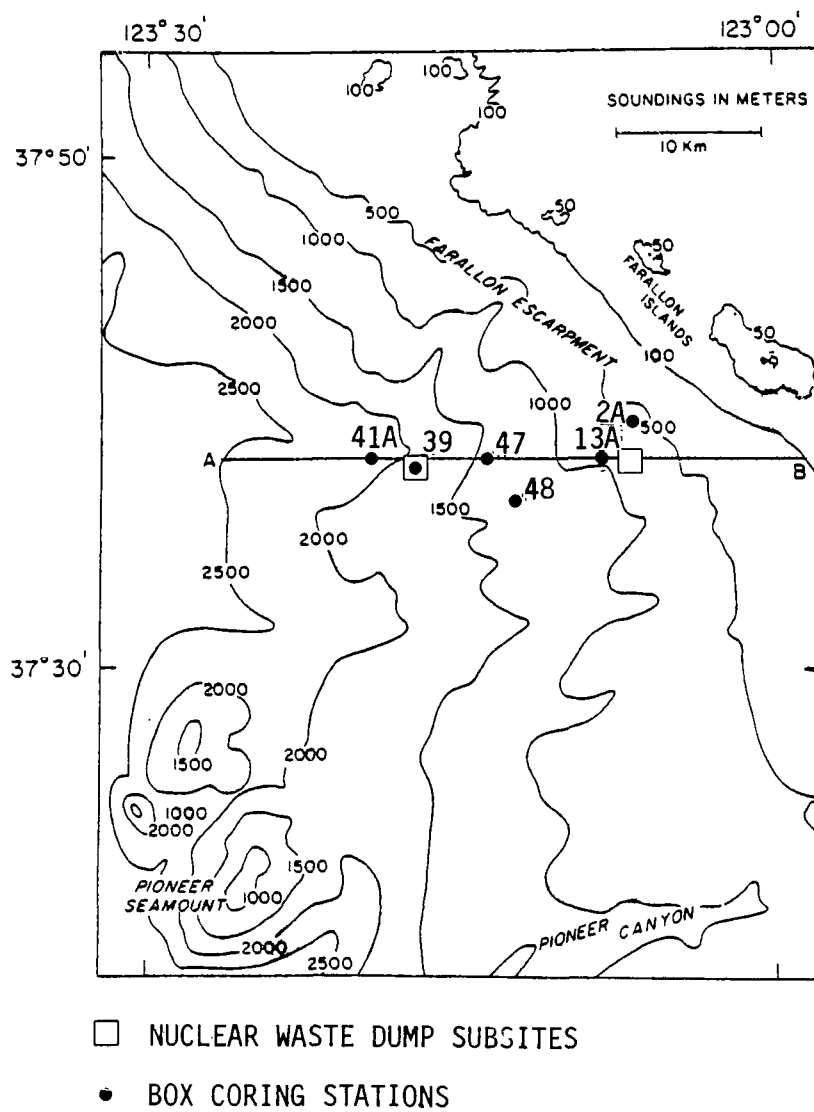
3.5 SEDIMENT INFORMATION

During August and September 1977, six box cores were collected for sediment analysis [3]. The locations of those coring sites are shown in Figures 3-5 and 3-6 and Table 3-3. The sample at Station 41A was not fully recovered because the jaws of the box core did not fully close during retrieval.

Table 3-3. Box cores collected for sedimentological studies during R/V VELERO IV cruise (August-September 1977)

Station	Coring Date	Latitude	Longitude	Water Depth (m)	Total Recovery (cm)
13A	8/31/77	37°38.1'N	123°08.0'W	1042	33
2A	8/31/77	37°39.8'N	123°07.1'W	878	60
47	9/1/77	37°38.3'N	123°14.0'W	1335	34
39	9/1/77	37°38.0'N	123°17.0'W	1469	37
41A	9/1/77	37°38.0'N	123°20.7'W	2350	surface grab
48	9/1/77	37°36.6'N	123°12.7'W	1216	45

Sediment subcore samples were obtained from each of the box cores (except Station 41A) and were investigated for sediment properties, x-radiographic properties, and radiochemical properties. See [3] for the procedures followed to obtain and analyze the samples.



AB IS AN EAST-WEST TRANSECT AT NORTH LATITUDE 37° 38'

Figure 3-5. Locations of Core Sample Sites [3].

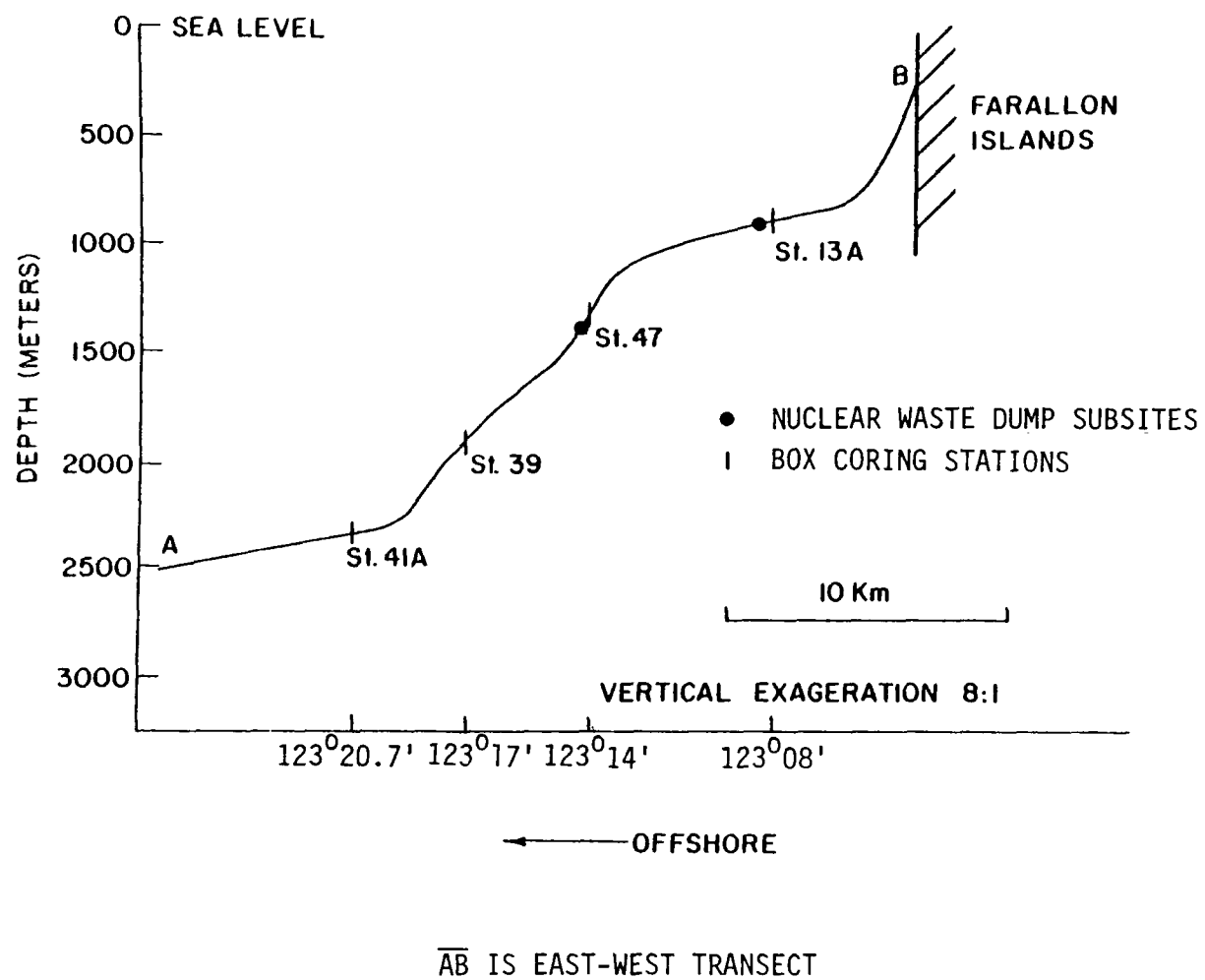


Figure 3-6. Depth Profile of Core Sample Sites [3].

4. DATA REDUCTION

In this section the data reduction for the current meters is described through the initial stages of processing, and the quality of the resulting data is assessed. Steps taken to improve the quality of the data are also described.

4.1 CURRENT METER DATA

The initial processing of the current data was accomplished in five stages: (1) data tapes were translated into a computer-readable digital format, (2) data tapes were checked for format errors such as missing bits in a word, missing words in a record, or missing records (these errors were then flagged for later processing), (3) digital counts from the translated data were converted to metric engineering units, (4) data in engineering units were checked for physically unreasonable values, and (5) both format errors and physically unreasonable data were removed and replaced by linearly interpolated values.

When the resulting data were examined it was found that Aanderaa meters 2830 and 2920 contained a large amount of unexplained scatter and were deemed unsuitable for analysis. In an attempt to recover the data the raw binary data tapes from these meters were examined with an oscilloscope. It was found that the pulse widths for the binary ones and zeros varied beyond manufacturer specifications during the record. However, the ratio of the pulse widths to the time between the trailing edges of consecutive pulses remained constant. The tapes for meters 2830 and 2920 were then retranslated using this ratio to distinguish between ones and zeros in the record. In this way, it was possible to recover the data for the entire period of record for both current meters.

Verification of the current meter data in terms of relative calibration and timing accuracy is discussed in Section 5.2.

4.2 GENERATION OF BATHYMETRIC CHART

The bathymetry obtained was annotated to the ship's position at the time of deployment, and the resulting position and depth coordinates were compared with those found on an oceanographic data chart, "LBL Publication 92," produced by the Lawrence Berkeley Laboratory ^[4], and with bathymetric data from previous surveys in 1974 and 1975. The bathymetric measurements taken during the deployment of the meters

generally corroborate the larger features depicted on published bathymetry. However, smaller features were observed in the local bottom terrain which are not shown in the standard publications. This situation was also observed with regard to the soundings taken during the 1975 survey. The soundings performed in 1977 indicate the presence of an east-west running depression as shown in Figure 2-1. A section of the LBL chart has been reproduced and is shown in Figure 4-1.

4.3 GRAIN SIZE FROM SEDIMENT SAMPLES

The tube cores (subcores) described in Section 3.5 were separated by 2-millimeter and 63-micrometer sieves to determine the percentages of sand, silt, and clay. Sand is defined as being composed of particles between 2 millimeters and 63 micrometers in diameter, while silt and clay are less than 63 micrometers in size.

Cumulative probability distributions of grain size were obtained for each of the sampling stations (see [3]). Statistical parameters, including mean, median, standard deviation, skewness, and kurtosis were obtained for each distribution as a function of depth beneath the bottom surface in order to determine the cross-sectional profile of the sediments. This information is used in Section 6.2 for determination of transport potential from the site.

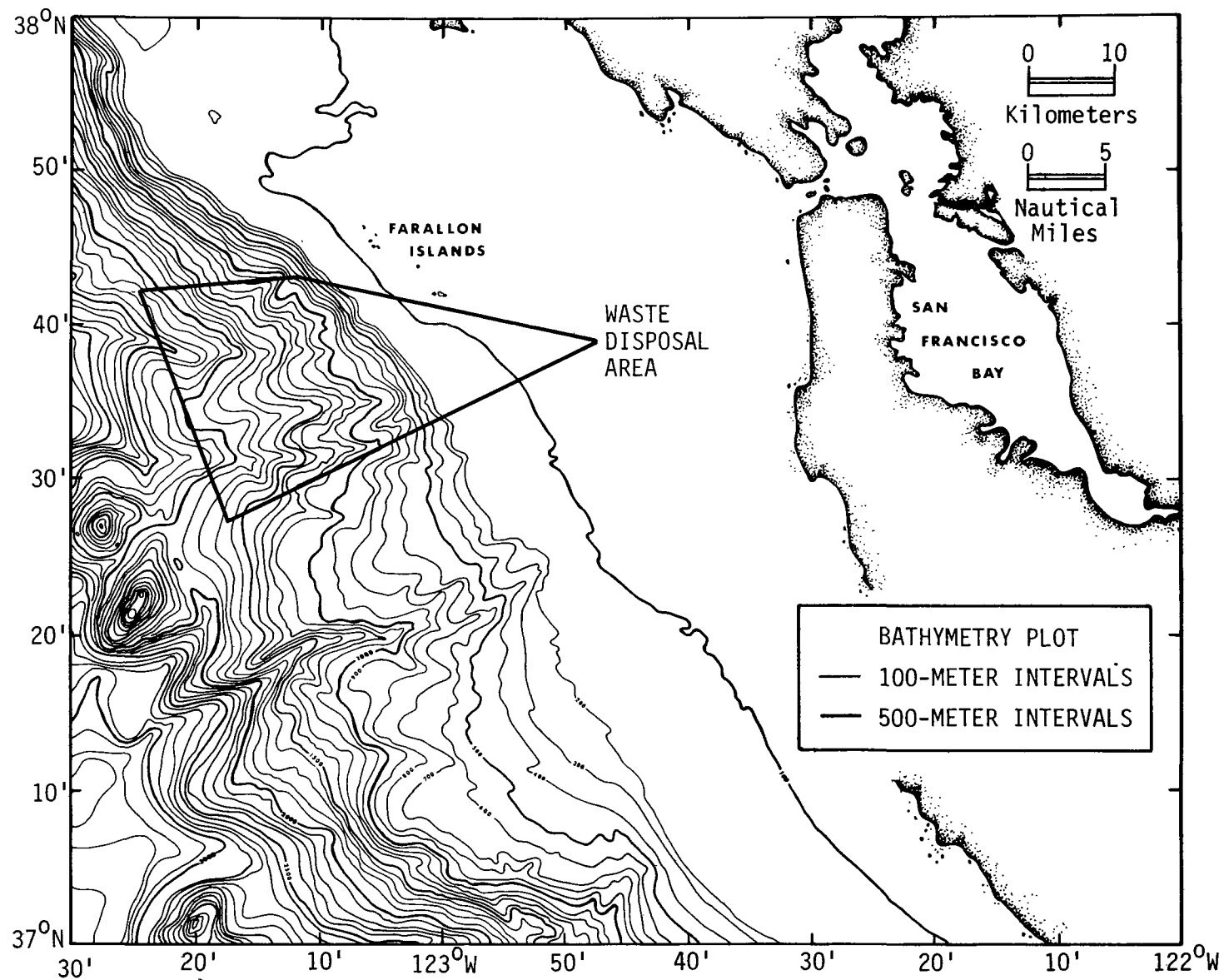


Figure 4-1. Bathymetry Chart [4].

5. CURRENT METER DATA PROCESSING

This section describes the processing and verification of current meter data that were performed prior to interpretation. The data from each meter were separated into data sets after preparation (e.g., translation, conversion, editing, and interpolation) described in the previous section. The processing consisted of applying various statistical algorithms to the data in both the time and frequency domain. The output consisted of time history plots, histograms, scattergrams, progressive vector diagrams, stick plots, power spectral density plots, and listings of summary statistics.

5.1 DATA PRODUCTS

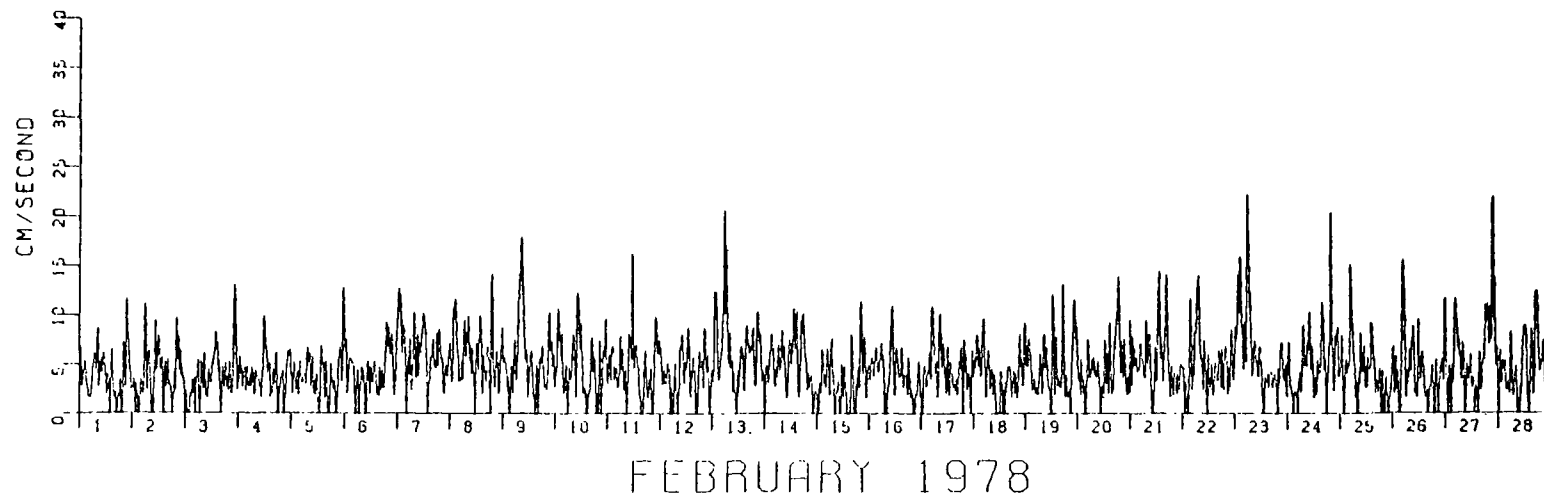
Various statistical functions were performed on the data to examine different aspects of current conditions at the site. Time history plots chart continuous measurements of current flow and direction; histograms and scattergrams provide individual and combined distributions of the measured quantities; power spectra show periodic components in the data; and progressive vector diagrams and stick plots illustrate the long-term average components in the data.

Definitions and samples of the data products prepared from the reduced data are given below. A complete set of plots and tables are contained in the Appendices.

5.1.1 Time History Plots of Current Speed and Direction

Monthly plots are included for each current meter on a horizontal scale of 1 day per division. Speed is plotted on a scale of 5 cm/s per division from 0 to 40 cm/s, and current direction is plotted on a scale of 45 degrees per division. To aid in the interpretation of current directions, the pen was lifted whenever two consecutive current directions differed by more than 180 degrees, with the assumption that the current vector went through 0 degrees (True) between these readings (e.g., for three successive readings of 359°, 0°, and 1°, the pen would be up between the first and second point, but down between the second and third). A reading of 0 degrees (True) for current direction implies that the current is moving toward true north, while 45° corresponds to northeast, etc. A sample plot for February 1978 is given for Aanderaa meter # 2920 in Figure 5-1. The average velocity for this sample is approximately 4 cm/s, with a mildly predominate northeast direction. The complete set is provided in Appendix A.

AANDERAA #2920
TIME HISTORY PLOT CURRENT SPEED



AANDERAA #2920
TIME HISTORY PLOT CURRENT DIRECTION

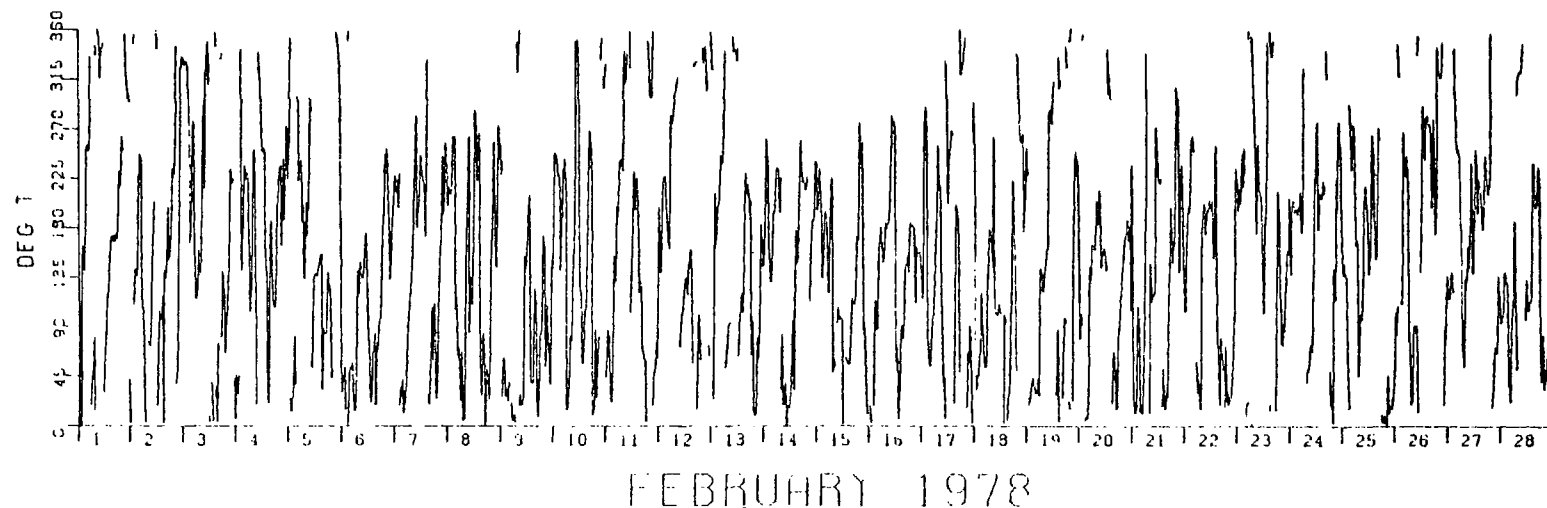


Figure 5-1. Time History Plot, Current Speed, and Direction
(Meter No. 2920)

The time history plots provide a quick and complete visual summary of the activity of the recorded data over the extent of the plot. Both long-term and short-term trends are visible in the display and implications can be made concerning the periodicity, stationarity, ergodicity, and overall quality of the data. Periodicity may be defined as the degree to which the time history is composed of periodic events. Stationarity and ergodicity are closely allied concepts. A data set may be considered stationary if its statistical properties (i.e., mean, variance, etc.) do not exhibit significant trends with time, and it is ergodic if the statistical properties of its data subsets do not significantly differ for different subsets. Stationarity and ergodicity are necessary preconditions for spectral analysis. Visual inspection can frequently be used to pick out questionable data records (such as excessive values represented by spikes) and locate places where there was a sensor failure (flat spots in the data or unexplained changes in the character of the time series).

The plot of current speed in Figure 5-1 clearly shows the tidal periods in the data and also shows that the data are reasonably stationary and ergodic. The data is evidently of good quality, as there are no unexpected changes in the overall appearance of the plot. Peak events are visible on the 9th, 13th, 23rd, 24th and 27th of the month. The direction time series shows evidence of the tidal rotation in the corkscrew appearance of the data (i.e., the way it appears to increase through a 360° range with the passage of time).

5.1.2 Time History Plots of U and V Current Components

The current speeds and directions are also represented in U (eastward-flowing) and V (northward-flowing) components. The plots are provided on a horizontal scale of 1 day per division and a vertical scale of 10 cm/s per division. The U and V components are derived as follows:

$$U = S \sin(a)$$

$$V = S \cos(a)$$

where

$$U = \text{East component (cm/s)}$$

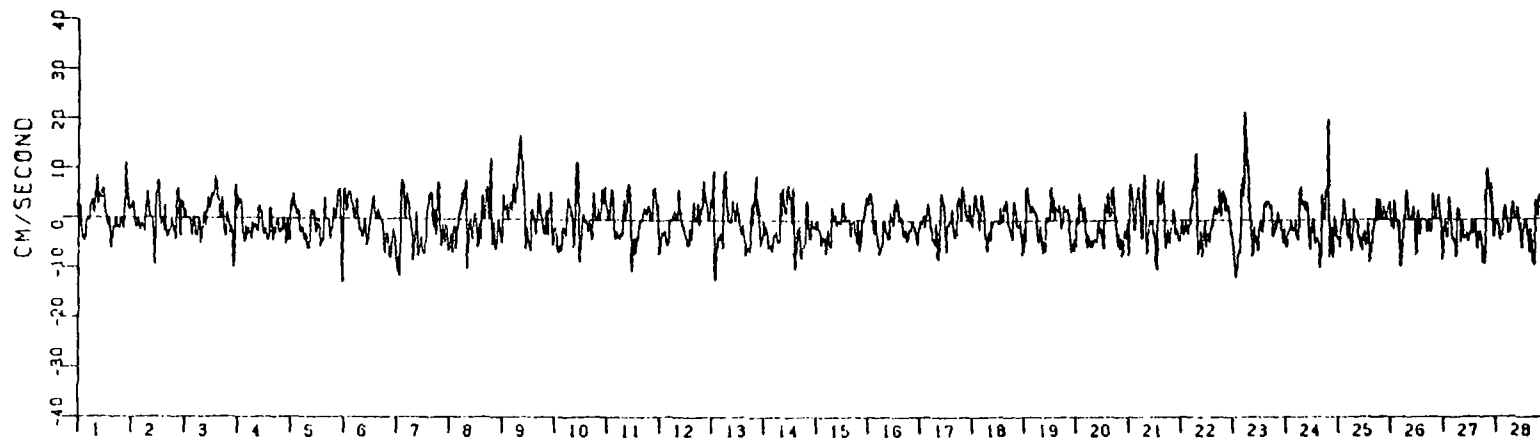
$$V = \text{North component (cm/s)}$$

$$S = \text{Current speed (cm/s)}$$

$$a = \text{Current direction (degrees true)}$$

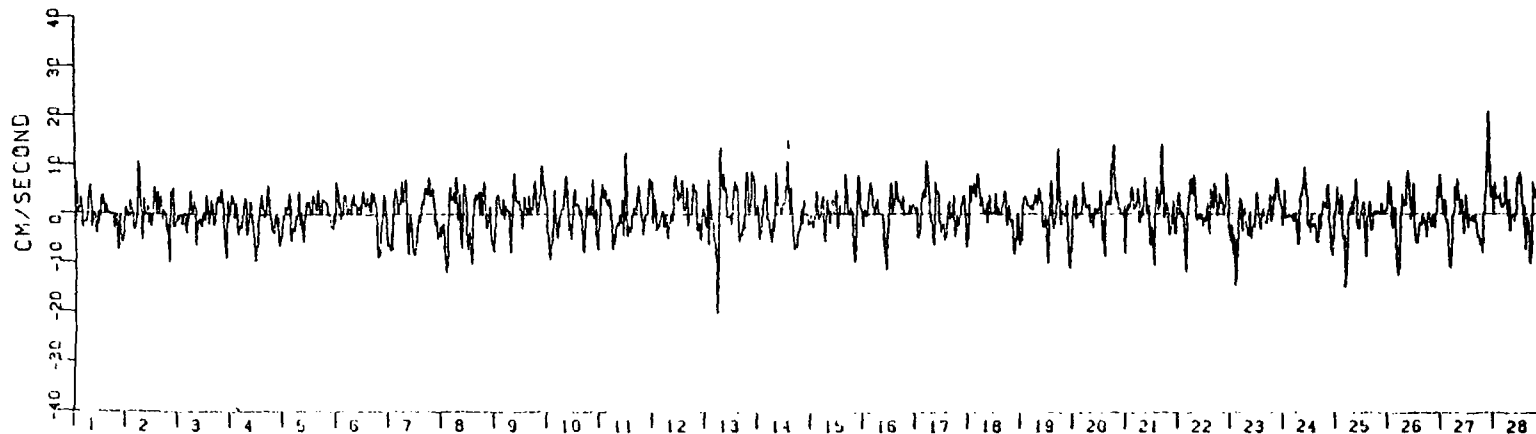
A sample plot for February 1978 is given for meter # 2920 in Figure 5-2. The complete set is contained in Appendix B.

AANDERAA #2920
TIME HISTORY PLOT NORTH CURRENT



FEBRUARY 1978

AANDERAA #2920
TIME HISTORY PLOT EAST CURRENT



FEBRUARY 1978

Figure 5-2. Time History Plot, North Current, East Current
(Meter No. 2920)

These plots corroborate the speed and direction plots by showing the tidal periods as before, and by revealing no abrupt changes in statistical character and no nonstationary processes. The currents appear to be more or less symmetrical with respect to direction, showing that the predominant factors affecting current are periodic in nature. Tidal influences seem to prevail in these plots. These observations are supported by inspection of the associated power spectral density plots (see Section 5.1.5).

5.1.3 Histograms

Histograms for each meter are included to provide the distributions of the measured quantities over the entire period of record. The following histograms were calculated:

Current speed using 2.0 cm/s intervals

Eastward (U) current component using 4.0 cm/s intervals

Northward (V) current component using 4.0 cm/s intervals

Conductivity (for meter # 2920 only) using 0.02 millimho intervals

A sample histogram of current speed for meter # 2920 is given in Figure 5-3. The complete set is contained in Appendix C.

The frequency histogram displays the frequency of occurrence within specified class intervals for the parameter shown in the headings. The class intervals are along the horizontal axis, with the frequency of occurrence within each interval shown on the vertical axis. The lower bound for each interval is greater than or equal to the value for the class, and less than the value of the next higher class (i.e., the histogram for speed is in 2 cm/s intervals and interval class "10" represents all the occurrences of speed greater than or equal to 10.0 cm/s and less than 12.0). Note that this representation will make a distribution appear to shift to the left by half a class interval.

Actual frequency for each interval is listed vertically in the heading above the interval. The total number of events (in this case 10154) is found to the right of the heading. The resolution of the frequency bars is variable depending on the data being plotted. The frequency scale is adjusted to give maximum resolution on each plot. Data flagged as erroneous are not counted in any interval or in the total number of events.

The histogram of Figure 5-3 assumes the general form expected for a non-negative parameter such as speed. The histogram is skewed towards the origin, or zero interval class (where 1500 events out of 10154 are observed), and displays a gradual taper towards the higher amplitudes to the right. There are no isolated events in the higher class intervals, suggesting that there are probably no unreasonable spikes in the corresponding time series plot.

5.1.4 Scattergrams

Scattergrams for each meter are included to provide joint distributions of measured quantities taken over the entire period of record. The following scattergrams were calculated:

Current speed versus current direction with speed binned at 2 cm/s intervals and direction binned at 18 degree intervals.

Northward (V) versus eastward (U) current components with both components binned at 4 cm/s intervals.

A sample plot of current speed versus direction for meter # 2920 is given in Figure 5-4. The complete set is contained in Appendix D.

The scatter diagram is a two-dimensional histogram that tabulates the number of occurrences of specified combinations of two variables. When the number of events in each box is divided by the total number of observations, the result may be interpreted as the joint probability density. The class intervals are indicated on the ordinate and the abscissa. The size of the matrix is limited to 20 by 20. The range for each interval is limited to integer values. Data flagged as erroneous in either of the variables causes the occurrence to be dropped from the calculation. The total number of correct occurrences represented in the diagram is printed at the top of each diagram.

Scattergrams can be used to assess the degree of statistical dependence of two measured parameters. The scatter diagram of Figure 5-4 shows the relationship of current speed to current direction for meter # 2920. It is apparent that the greatest current speeds occurred when the current direction was north, and no currents larger than 14 cm/s were observed with a southerly direction. The scattergram is smoothly distributed over the 360 degree range, and there are no speed/direction events isolated by more than one class interval from the distribution. There also are no conspicuous holes.

5.1.5 Spectral Density Plots of U and V Components

These plots were derived by the method of averaged periodograms from the U and V components of the current time series. The scale of the monthly spectral plot was determined by the peak spectral density in order to aid in the resolution of spectral peaks. The horizontal scale is frequency in cycles/hour and the vertical scale is spectral density in units of velocity squared times hours, where velocity is in cm/s. A sample plot for February 1978 is given for meter # 2920 in Figure 5-5. The complete set is contained in Appendix E.

INTERSTATE ELECTRONICS CORP.
OCEANIC ENGINEERING DIV.

ANAHEIM, CA (714) 772-2811

METER TYPE - RANDERRA RCM-5

INSTALLATION DATE 10/24/77 1940 HRS

POSITION 37 36 36.0N 123 7 32.1W

METER S/N - 2920

ANCHOR DN 35 HRS

METER REF - 749

ANCHOR RELEASE 620HRS

ANCHORED BUOY B

SITE DEPTH - 914 METERS

METER DEPTH - 911 METERS

RECOVERY 3/14/78 620 HRS

TIME ZONE - PDT (GMT +08 HRS)

SAMP INTV - 20 MIN

SCATTER DIAGRAM
NUMBER OF EVENTS PER MATRIX UNIT
SPEED VS DIR

TOTAL NUMBER OF EVENTS: 10154
FLAGGED DATA POINTS: 0

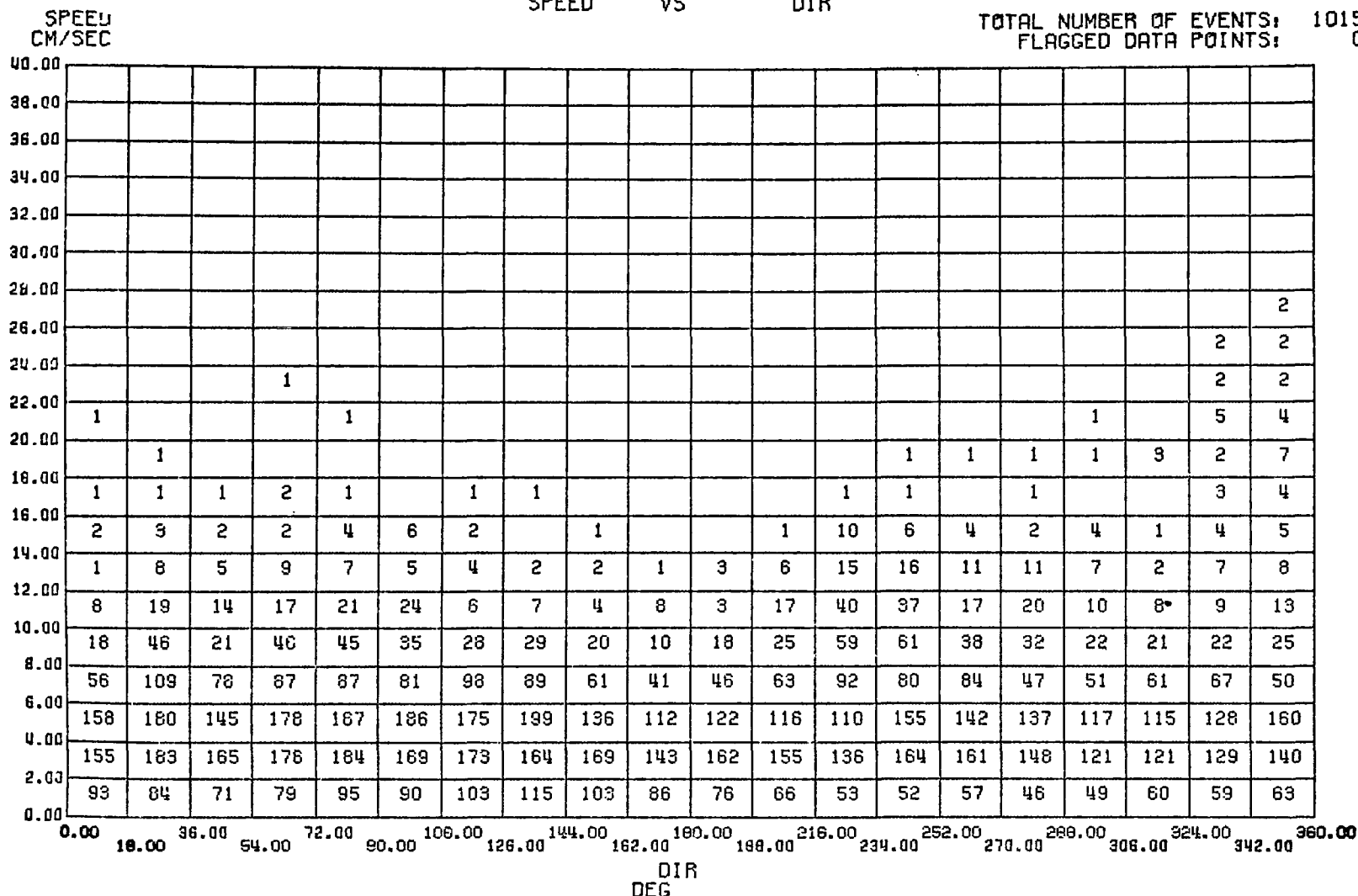
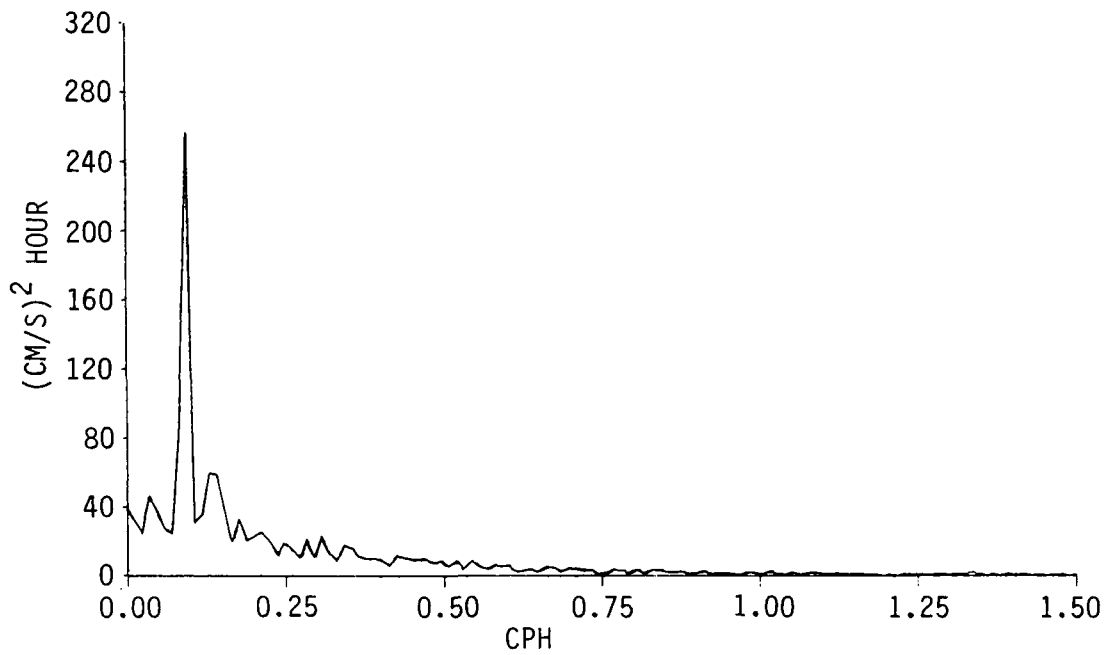


Figure 5-4. Speed Versus Direction Scattergram (Meter No. 2920)

NORTH CURRENT



EAST CURRENT

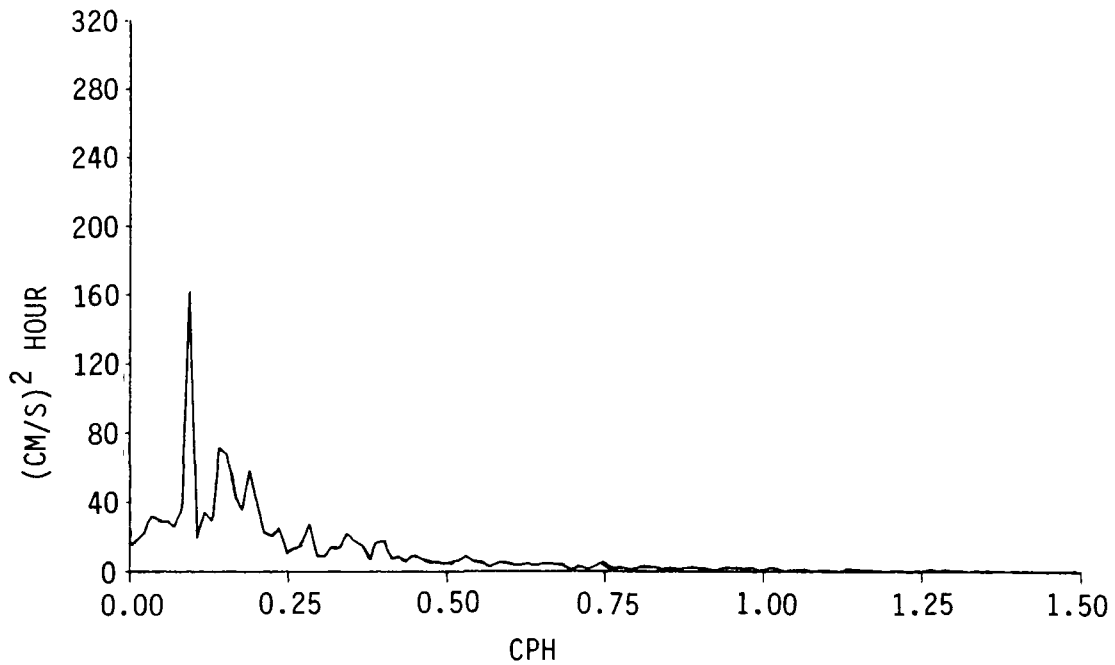


Figure 5-5. Power Spectrum (Meter No. 2920; February 1978)

The spectral density function of a parameter displays the amount of variance around the mean caused by components that occur with a regular frequency. Thus, it is a method of describing the mean square value or relative energy of a time series as a function of frequency. Periodic components of the data, such as diurnal and semidiurnal tidal currents, are represented by peaks in the frequency spectrum. The relative size of these peaks is an indication of the relative importance of the corresponding periodic process. Higher peaks demonstrate that more energy is contained in the measured parameter at the respective frequency.

The spectral density can be thought of as the Fourier transform of the autocorrelation function, and is calculated using standard FFT algorithms. Figure 5-5 clearly shows the spectral peak for the semidiurnal tides in both the east and north currents during February 1978. Some energy at higher frequencies is also visible, especially for the east current, but nothing significant exists at frequencies higher than 0.5 cycles per hour.

5.1.6 Progressive Vector Diagrams

Progressive Vector Diagrams (PVDs) are provided for each of the 5 meters showing the cumulative vector sums of the east and north current components over the life of the meter. The PVDs were calculated from time series of low pass filtered data in order to eliminate tidal variations from the plot, and give a smooth curve depicting long-term trends. Each of the east and north component time series were filtered with a cosine-tapered symmetric filter with a cutoff frequency of 0.020 cycles per hour (corresponding to a 50-hour period). The PVDs were then plotted to a uniform scale of 40 kilometers per inch. A sample plot is given in Figure 5-6 and the remaining plots are included in Appendix F.

PVDs provide a visual representation of the sequential current observations recorded by a current meter. Current speeds and directions are broken into their U and V components and are summed from consecutive data and plotted in vector form--tip to tail.

An important fact to remember when using PVDs, is that the instrument is fixed in space as it records current data. The vector sum of the components is not the path of a water particle through space, but rather the sum of instantaneous current measurements at one fixed point. The current velocity field must be determined from a sufficiently defined array of meters before water particle trajectories can be derived. However, a PVD can be used to support observations about current behavior in the immediate vicinity of the meter, or to compare measurements from separate locations. The PVD in Figure 5-6 for meter # 2919 shows the prevailing direction to be toward the north with a slight tendency to the east. The current vector is relatively straight, suggesting that a fairly steady residual (after removal of tides) current exists at this point.

FARALLON ISLAND CURRENT METER DATA
 BANDERAA METER # 2919
 OCT 25, 1977 - MAR 10, 1978

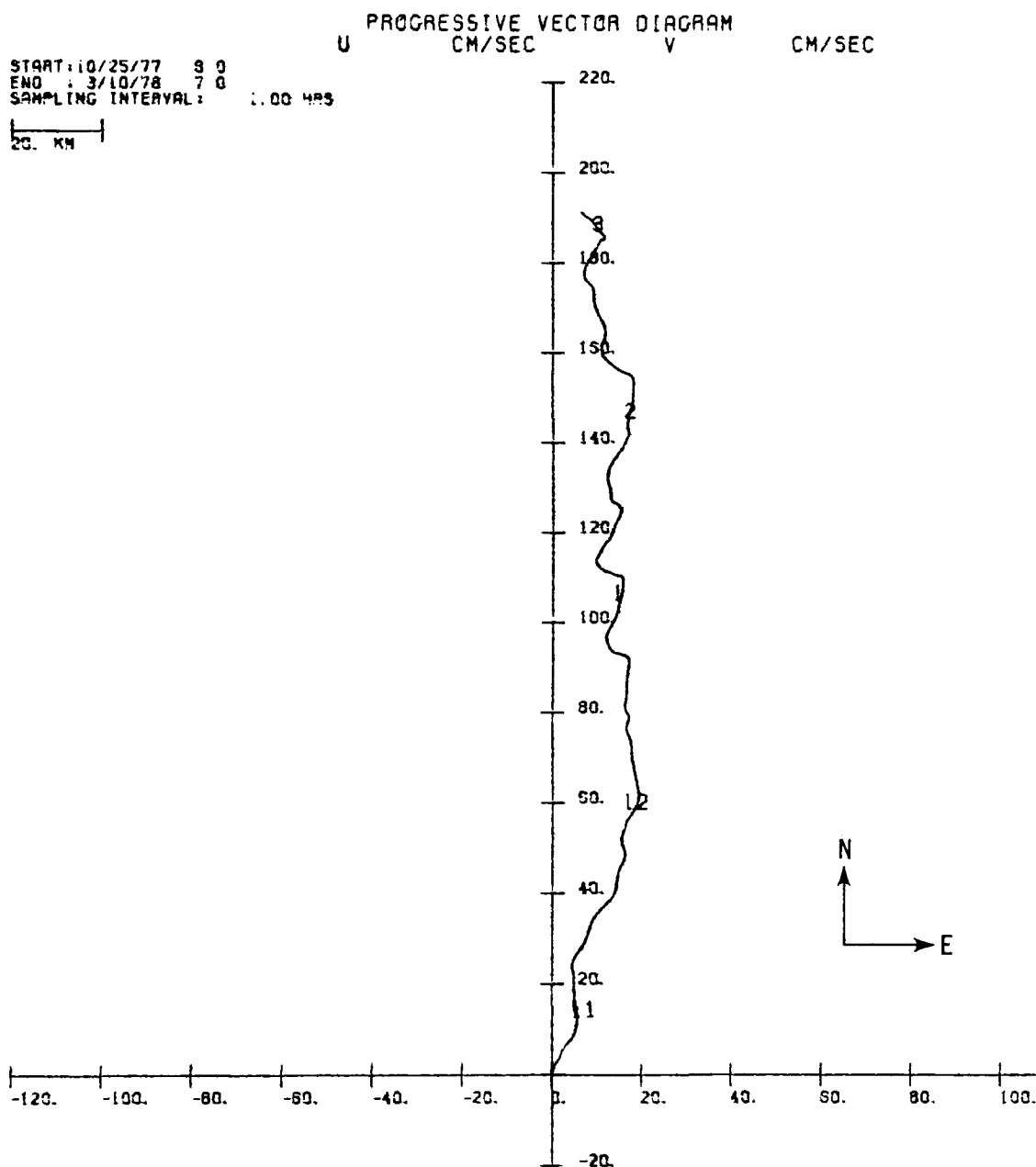


Figure 5-6. Progressive Vector Diagram (Meter No. 2919)

5.1.7 Stick Plots

Three-hour averages of speed and direction are plotted on a polar coordinate system that moves through time. Stick plots showing current speed and direction are included in Appendix G. The length of the vector represents speed, and the angle of the vector represents direction in the true geographic coordinate system (degrees of direction increase clockwise from north, which is vertically oriented on the diagram). Time is indicated along the bottom of the diagram. Plotted beneath each stick plot is a time series plot of speed for quick cross-reference. Peaks in the time series plot can be matched with their respective vectors on the stick plot.

The stick plot contains the same information as the PVD, except that the vectors are plotted on a horizontal scale instead of end to end. Figure 5-7 shows a stick plot for meter # 2918. Inspection reveals a wide range of scatter in both current magnitude and direction, but there appears to be a strong tendency for the current to travel east-west, as evidenced by the relatively shallow angle between the stick plot vectors and the horizontal axis.

5.1.8 Summary Statistics

Daily, monthly, and whole study summary statistics are compiled for each current meter. The statistics consist of mean, minimum, and maximum values, and also standard deviation (SIG), skewness (SKW), and kurtosis (KUR). These statistics are calculated for current speed and north (V) and east (U) current components. A sample listing of daily statistics for meter # 2919 is given in Figure 5-8. Note that the time given for each entry in the table is the time at which summary statistics were generated for all preceding data since the last entry. The remaining tabulations are included in Appendix H.

The summary statistics show the first four moments of the data distribution and can be used to assess data quality and stationarity. For stationary data the statistical properties remain constant over time. Consequently, if the statistical moments (mean, variance, skewness, and kurtosis) remain within reasonable ranges, the time series can be considered stationary.

The variance or the standard deviation provide measures of the dispersion of the data about its mean. An excessive degree of dispersion can indicate discontinuities in the time series, or bimodality in the distribution, while a very small dispersion (i.e., standard deviation approaching zero) may indicate the absence of a meaningful signal. This may occur in the event of a sensor failure.

The skewness represents the degree of asymmetry, or departure from symmetry, of a statistical distribution. If the distribution has a longer tail to the right than to the

AANDERAA METER #2918

SPEED STICK PLOTS DIR DEG

START: 12/25/77 555
 END: 12/20/77 15
 AVERAGING INTERVAL: 100.00 MIN
 10.00 CM PER SEC PER INCH

33

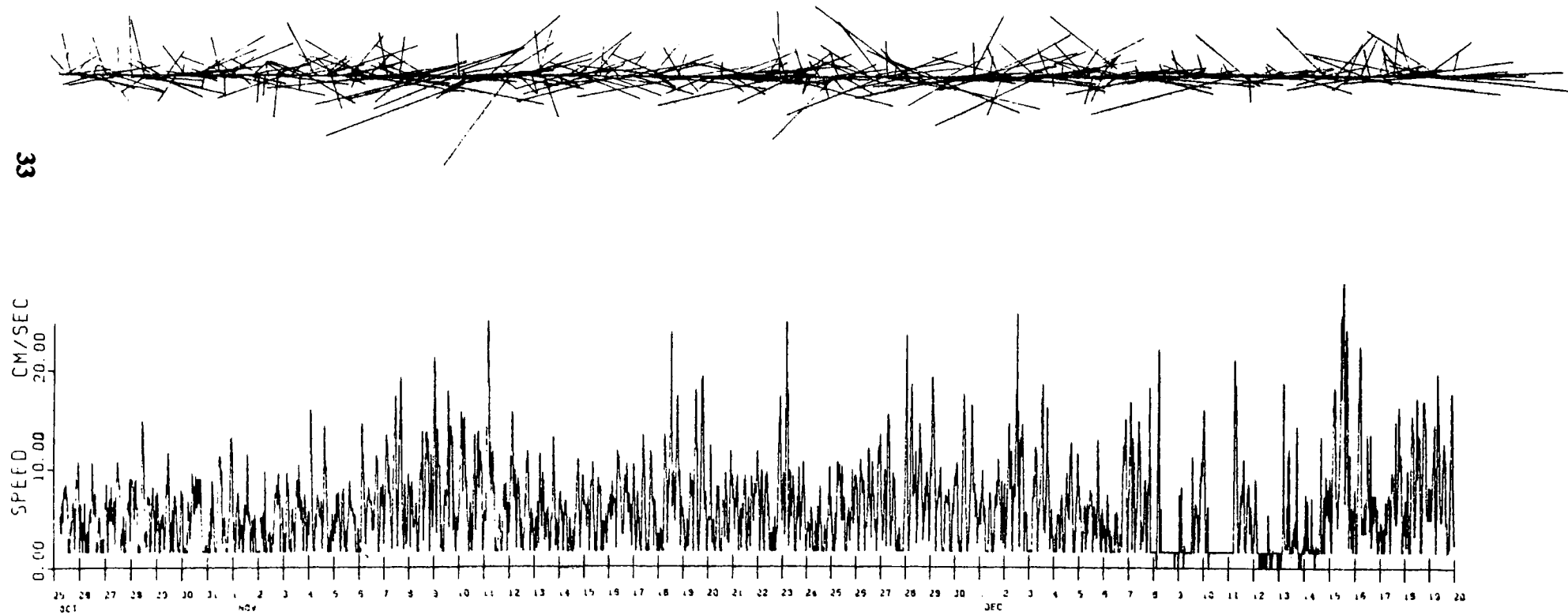


Figure 5-7. Stick Plot (Meter No. 2918)

INTERSTATE ELECTRONICS CORP.
OCEAVIC ENGINEERING DEV
ANAHEIM, CA (714) 772-2811

SUMMARY STATS FOR U

		START TIME: 10/25/77 05:55		- END TIME: 3/10/78 07:48						
		METER TYPE - AANDERAA RCM-5		METER # - 2919		SAMP INTV - 20 MIN				
	MNTH	DAY	YR	TIME	MEAN	MIN	MAX	SIG	SKW	KUR
1	10	26	77	8	.92	-7	10	5.06	.13	1.49
2	10	27	77	9	.23	-10	11	3.76	-.03	3.37
3	10	28	77	3	1.00	-8	12	5.56	.16	1.91
4	10	29	77	3	.14	-11	13	5.60	.29	2.52
5	10	30	77	9	1.70	-7	12	4.39	-.15	2.51
6	10	31	77	8	1.27	-7	7	3.66	-.50	2.17
7	11	1	77	8	2.00	-6	14	5.12	.55	2.30
8	11	2	77	9	-.69	-11	7	4.56	-.34	2.13
9	11	3	77	8	.47	-7	7	3.96	-.20	1.90
10	11	4	77	3	-.01	-10	17	5.86	.96	3.26
11	11	5	77	3	-.82	-10	9	4.92	.27	2.22
12	11	6	77	3	.70	-8	12	5.01	.13	2.03
13	11	7	77	3	-.04	-11	12	6.58	.24	1.59
14	11	8	77	3	-1.09	-22	18	8.68	-.08	2.54
15	11	9	77	3	.31	-20	12	8.12	-.56	2.29
16	11	10	77	3	-.52	-20	14	7.94	-.12	2.63
17	11	11	77	3	-.57	-20	12	7.29	-.76	3.25
18	11	12	77	3	.50	-9	8	4.24	-.28	1.97
19	11	13	77	8	1.00	-10	9	4.41	-.09	2.20
20	11	14	77	8	-.36	-11	8	4.40	.01	2.20
21	11	15	77	3	1.59	-7	9	3.97	-.22	2.26
22	11	16	77	9	2.15	-10	9	4.25	-.82	2.80
23	11	17	77	3	.76	-9	11	4.72	-.27	2.09
24	11	18	77	3	1.17	-12	11	5.19	.04	2.94
25	11	19	77	3	1.12	-14	14	7.29	-.29	2.19
26	11	20	77	3	1.21	-15	19	7.47	.16	2.51
27	11	21	77	3	1.15	-9	14	4.89	.13	2.39
28	11	22	77	3	2.43	-9	14	5.51	-.31	2.19
29	11	23	77	3	-.30	-22	13	8.06	-.93	3.36
30	11	24	77	8	.71	-8	9	4.03	-.04	2.32
31	11	25	77	8	.61	-7	3	3.96	-.06	2.19
32	11	26	77	8	.97	-14	11	5.90	-.63	2.57
33	11	27	77	9	-.82	-23	13	8.76	-.84	3.00
34	11	28	77	3	-1.07	-22	14	8.38	-.57	2.93
35	11	29	77	3	.71	-14	20	8.55	.35	1.87
36	11	30	77	9	.59	-16	8	6.31	-1.25	3.66
37	12	1	77	8	1.28	-9	19	5.43	.78	3.68
38	12	2	77	3	.90	-10	11	5.80	-.07	1.75
39	12	3	77	9	1.33	-19	13	7.33	-.64	2.80
40	12	4	77	3	.59	-15	12	6.52	-.69	2.91
41	12	5	77	3	.97	-8	11	5.19	.07	1.74
42	12	6	77	3	-.15	-8	10	4.42	.48	2.48
43	12	7	77	9	-.54	-18	12	7.25	-.08	2.08
44	12	8	77	3	-.48	-18	16	8.57	-.01	2.09
45	12	9	77	9	-1.54	-26	19	3.77	.25	3.52
46	12	10	77	8	.57	-22	14	7.23	-.73	3.35
47	12	11	77	9	-.98	-26	14	8.57	-.90	3.39
48	12	12	77	3	-.93	-25	14	9.45	-.71	2.90
49	12	13	77	3	.00	-25	15	9.68	-.98	3.48

Figure 5-8. Summary Statistics (Meter No. 2919)

left of its mean, it has a positive skewness. Likewise, it has a negative skewness if the distribution is slanted to the left. Quantities which are expected to follow a Gaussian distribution, such as the east and north current components, tend to exhibit little skewness. Current speed, on the other hand, should tend towards a positive skewness since the distribution is bounded on the left by zero.

The kurtosis is a measure of the degree of peakedness of a distribution. The normal distribution has a kurtosis of 3. A distribution with a steeper peak has a higher kurtosis and is called leptokurtic. A low kurtosis, corresponding to a platykurtic condition, is indicative of a relatively flat-topped distribution. A failed sensor can frequently be identified by the presence of a leptokurtic condition in the measured data since, in this case, the measured signal will frequently assume a constant or near constant value. Platykurtic data may indicate bimodality in the distribution.

The minima and maxima are useful in isolating extreme events for closer study, and may also be used to corroborate the amount of dispersion indicated by the standard deviation.

Figure 5-8 lists daily summary statistics for the east current from meter # 2919. Based on the physical nature of the data, the east current would be expected to follow a more or less Gaussian distribution, and a glance at the tabulated values of kurtosis, which range between 1.49 and 3.68, suggest a mild degree of platykurtosis. There is also a degree of negative skewness, indicating the presence of a slant towards the right. This observation is verified by the frequency histogram (Appendix C). Consequently the PVD for meter # 2919 might be expected to occupy the first or fourth quadrants, and it does in fact does occupy the first quadrant.

5.2 VACM AND AANDERRA COMPARISON

The VACM and Aanderra meter # 2830 were located less than 1 meter apart on the same string and were almost 0.5 kilometer above the bottom. These two meters were compared by looking at the gain and phase transfer functions between their respective speed measurements. Since the meters had different sample rates, the VACM output was interpolated to give equivalent sample rates for comparison. In the ideal case when the meters measure exactly the same phenomena, the transfer function magnitude would be equal to one at all frequencies. The phase angle would show any lead or lag between the meters for different frequencies, and would be linear.

Prior to calculating the transfer function between the two meters, the lower order statistical functions were reviewed to determine how closely the statistical parameters were in agreement. It was discovered that the PVDs were not in agreement, and that the

VACM data was displaced in time relative to the Aanderaa meter by more than 2 months. Close visual inspection of the two sets of time series indicated that the two meters were measuring the same events over the following intervals:

Aanderaa # 2830

10/25/77 4:22
2/06/78 23:42

VACM

1/09/78 16:41
4/24/78 21:06

It is possible to visually match these two data records on a peak-by-peak (and indeed almost a point-by-point) basis.

Thus, it is apparent that at least some of the VACM data was transposed in time. Evidently, at some point during the initial handling and transcription of the raw VACM data tape, portions of the data record were processed out of sequence, and the altered data sequence was retained during all subsequent processing until its discovery during the analysis described in this report. Further scrutiny of the VACM's PVD revealed the presence of many unaccounted for cusps in the progressive vector path, suggesting that these might be break points where transpositions occurred. Efforts were made to reconstruct the correct sequence of data by examining the data around the cusps and matching trends with data beginning or ending at other cusps. Each of the reconstructions began with the portion that matches the PVD of meter # 2830. In Figure 5-9, a new PVD was constructed by removing the known out-of-sequence data segment at the beginning of the record to the end of the record while leaving the remainder of the sequence intact. In Figure 5-10, an effort was made to match the directions of the low-pass filtered data on either side of the cusp. Figure 5-11 was constructed in the same manner, but using unfiltered PVD segments so that short duration direction trends could be matched. Figure 5-12 was made by observing the visual record of spring and neap tides in the unfiltered PVD sequence, and attempting to construct a logical sequence from these observations. No one single reconstruction presented itself as being indisputably correct, and several possible alternatives are shown in Figures 5-9 through 5-12. Note that all of the reconstructions, as well as the original PVD, result in a markedly eastward vector average.

In accordance with the above findings, the comparison between meter # 2830 and the VACM used the 104-day stretch of VACM data starting on January 9, 1978. It was possible to visually identify corresponding events in the two sets of series, so a timing comparison was made between the two meters by matching peaks visually and comparing elapsed times since the beginning of the record. This leads to the observation that, although the relative drift was approximately 17 minutes for the last 80 percent of both records, the VACM appeared to lag behind meter # 2830 by around 9 hours for the first 20 percent of the compared intervals. Visual inspection of the speed time series for meter # 2830 suggests that there are gaps in the beginning of its data.

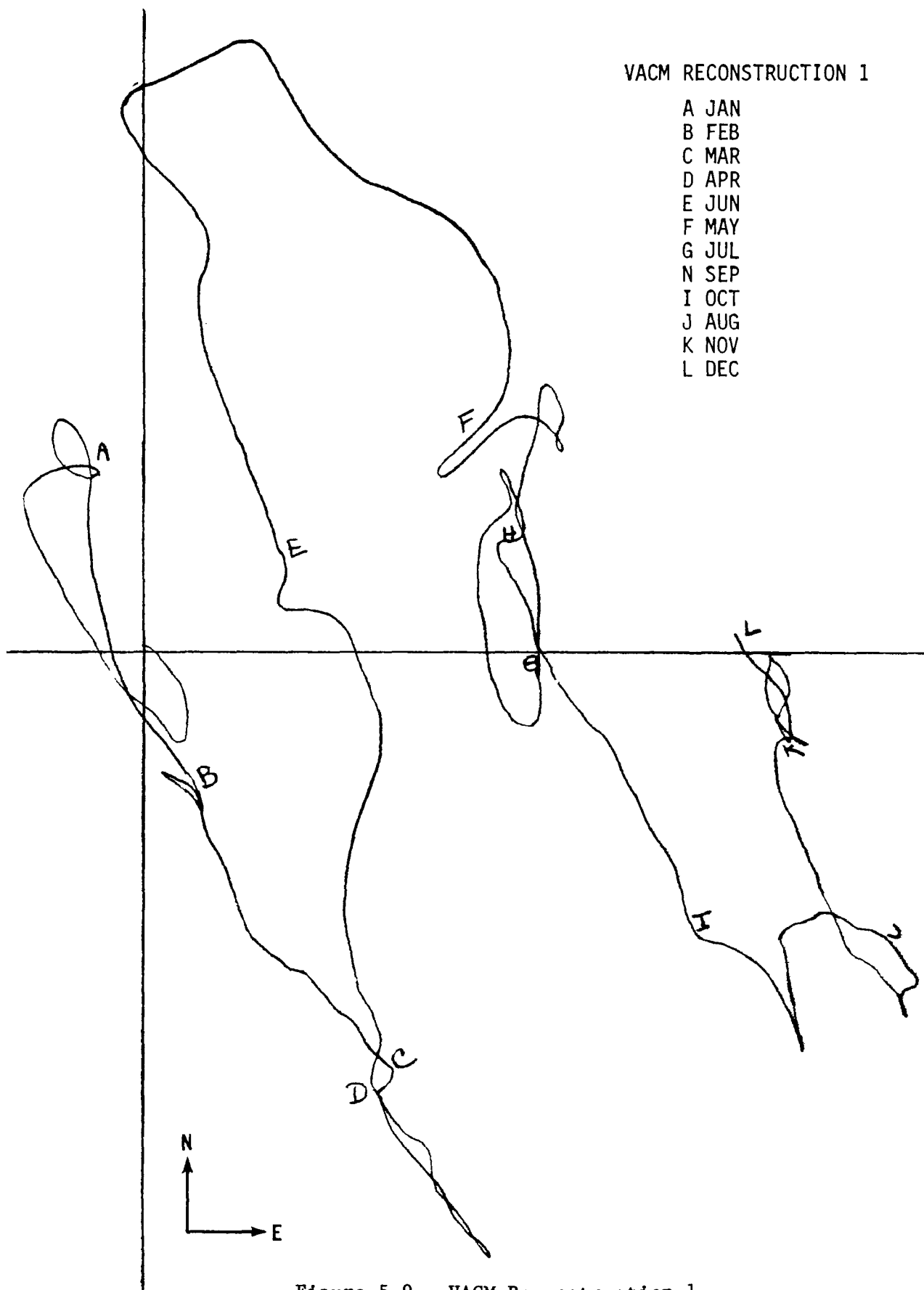


Figure 5-9. VACM Reconstruction 1

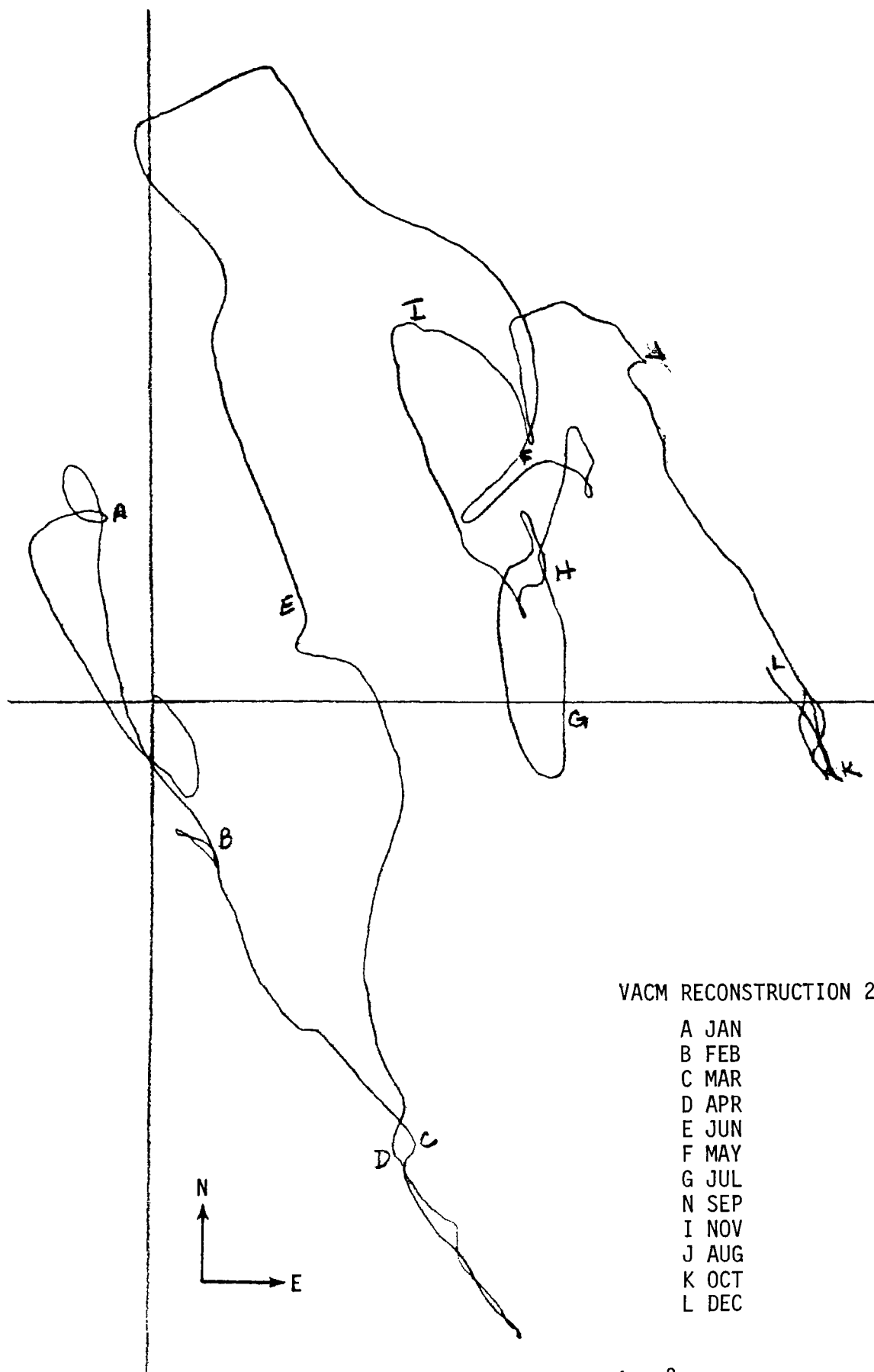


Figure 5-10. VACM Reconstruction 2

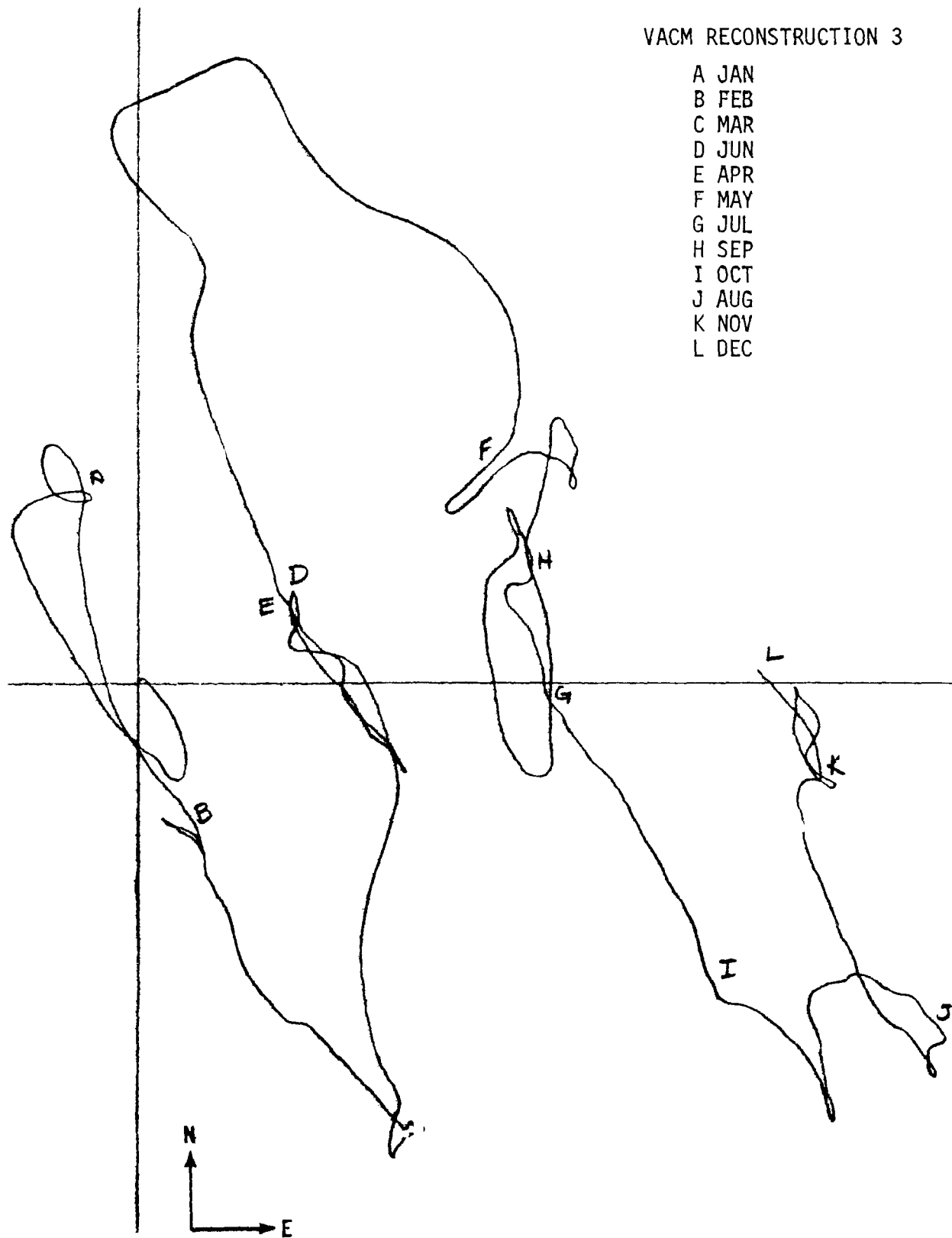


Figure 5-11. VACM Reconstruction 3

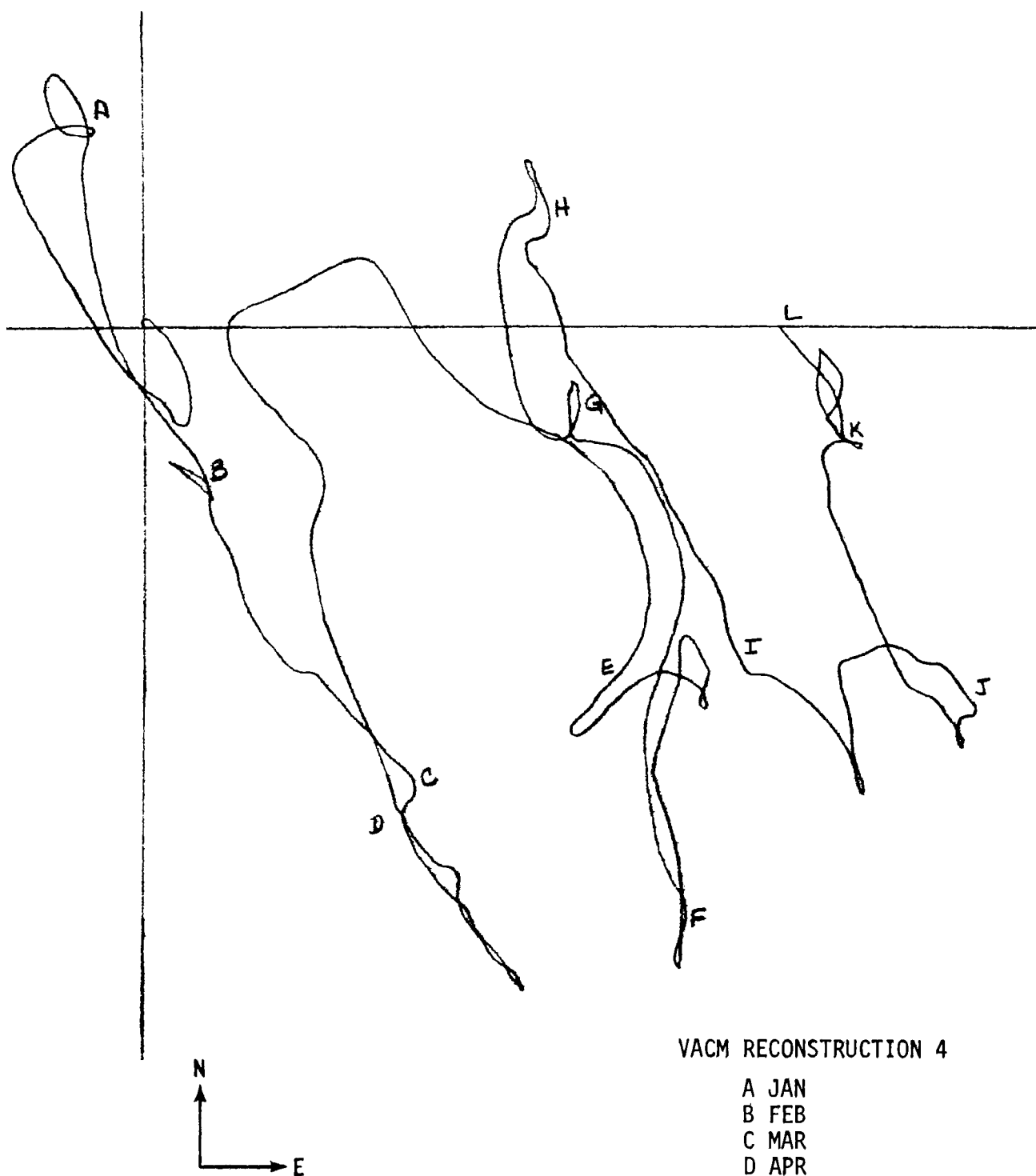


Figure 5-12. VACM Reconstruction 4

The speed transfer function was obtained between meter # 2830 and the VACM by # 2830/VACM. The unfiltered time series were used so that high-frequency events would be retained in the comparison. The gain and phase functions are shown in Figures 5-13 and 5-14, respectively. It is seen that the speed transfer function is fairly flat and within a range of 0.8 to 1.05, with the VACM generally giving a larger magnitude than # 2830. The phase portion of the transfer function is linear, indicating no substantial timing rate shifts between the two meters. This is the type of gain and phase relationship that should exist between similar sensors measuring the same parameter under equivalent conditions.

5.3 MEASUREMENT ACCURACY AND TIMING ERRORS

The main known phenomenon in the current measurement field is the occurrence of tides. All of the current measurements contained a significant amount of tidal energy at approximately 12-hour intervals. This information was used to determine timing errors. Once it had been determined with an initial inspection of the time series that there were no gross timing errors other than the one described for the VACM in the previous section, meter timing was evaluated by locating tidal peaks and comparing elapsed time since meter startup with the time obtained by multiplying the tidal period by the number of elapsed tidal periods.

Semidiurnal tides contain two major frequency components, one due to the gravitational influence of the moon, the other due to the pull of the sun. The lunar component has a period of approximately 12 hours, 25 minutes and is the major component. The solar contribution has a 12-hour period and accounts for around 46.6 percent as much influence as that of the lunar tidal contribution. In accordance with these facts, the tidal peaks were assumed to be 12 hours 25 minutes apart and heavily contaminated by other frequencies, mainly the solar 12-hour tide.

Several tidal peaks were selected from the time series for each meter to establish clock drift as a function of time. Peaks were selected for incorporation into the timing calculation based on the following criteria:

only peaks which had the greatest speed magnitude in a given 24-hour period were selected; and,

these speed peaks were used only if they occurred simultaneously with the daily maximum for the east-west current component.

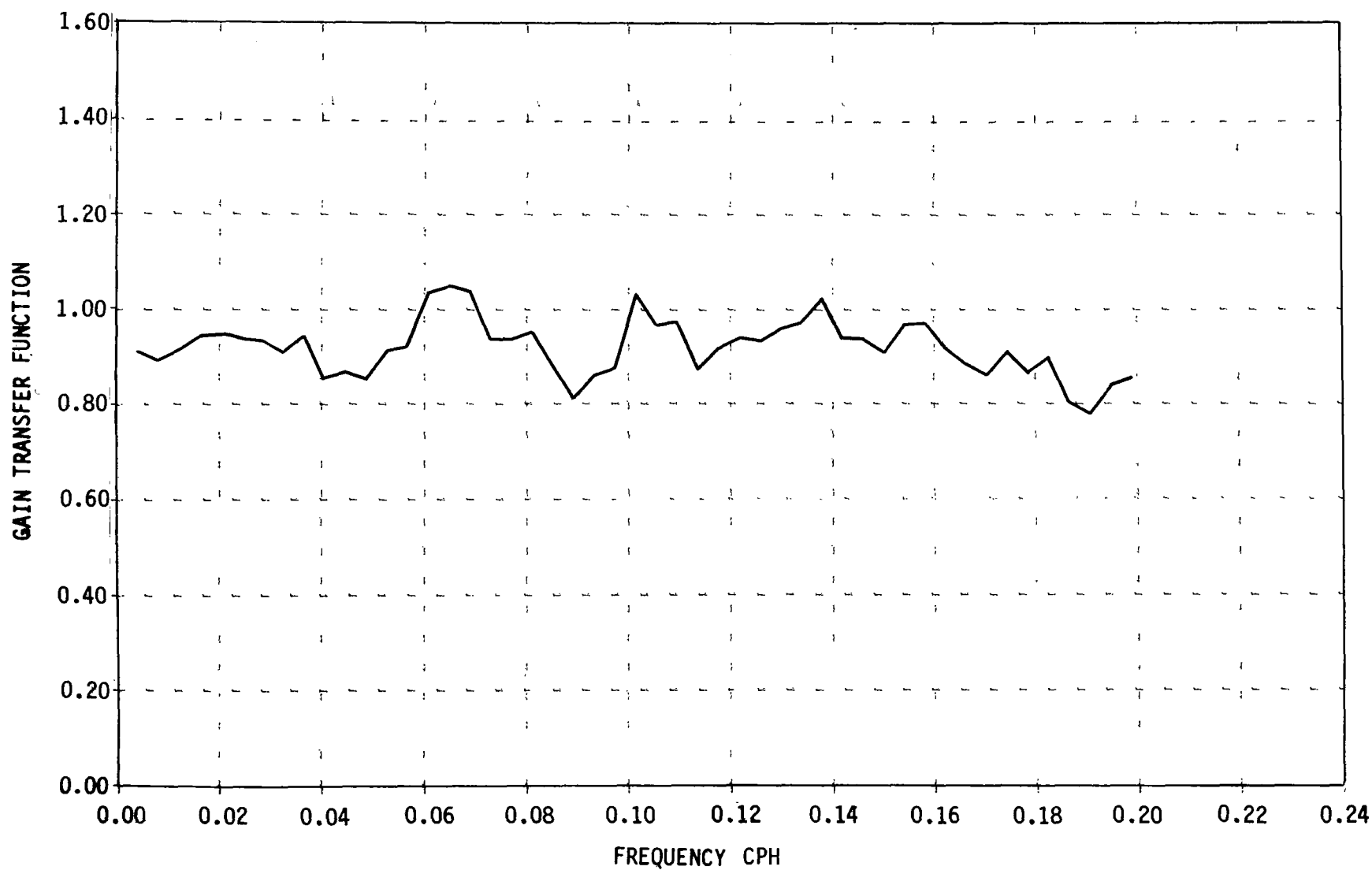


Figure 5-13. Speed Gain Transfer Function for Meter No. 2830 Versus VACM

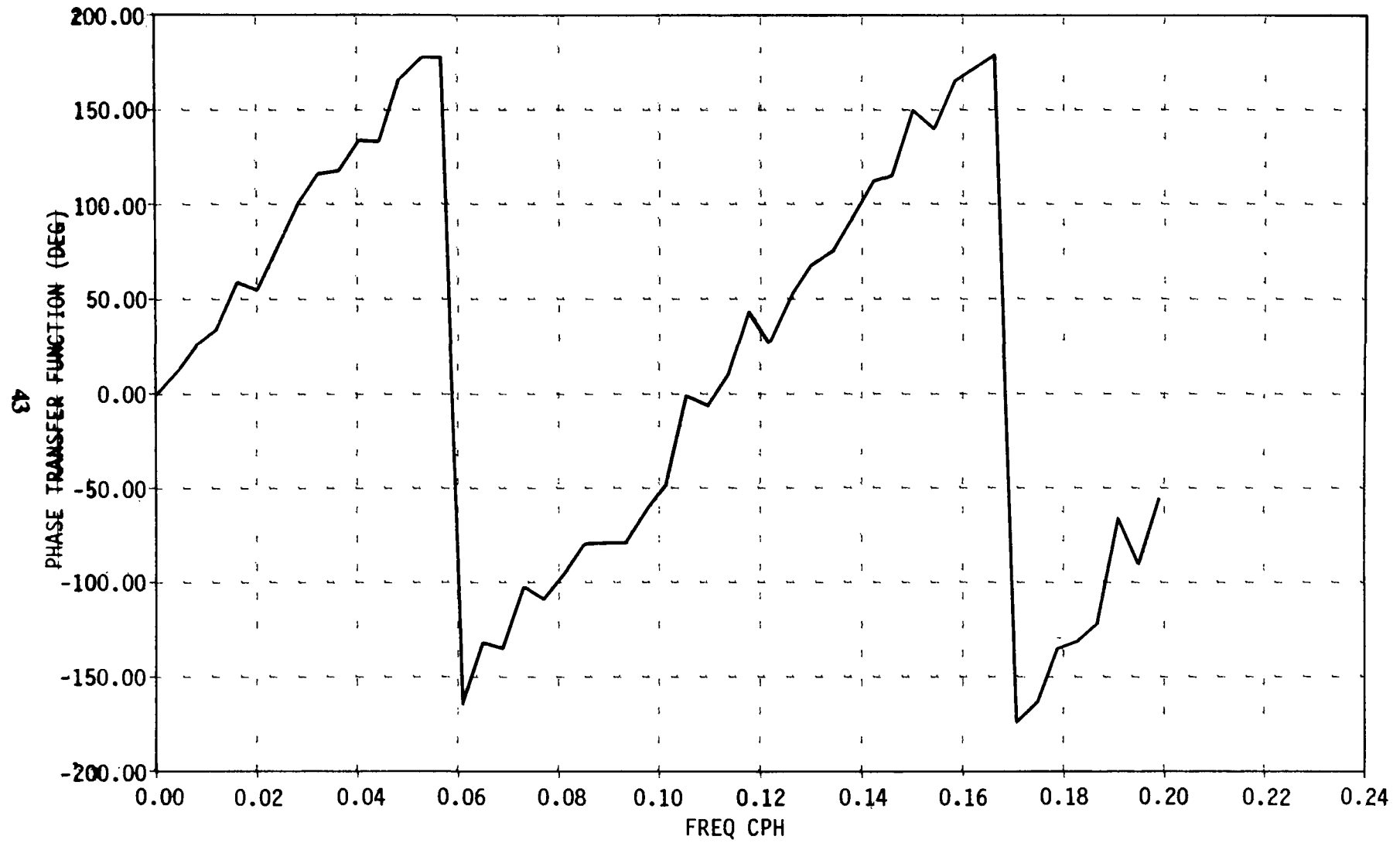


Figure 5-14. Speed Phase Transfer Function for Meter No. 2830 Versus VACM

A reference peak was chosen from the beginning of the time series, and the elapsed number of lunar semidiurnal periods (12 hours, 25 minutes) was calculated for each candidate peak with reference to the reference peak.

The calculated elapsed tidal intervals consisted of an integral number of periods plus some residual fraction of a period. Since the relative clock drift for each meter was found to be within one tidal period for each meter (see bottom of page 41) it was expected that the calculated residuals would be close to each other so long as the candidate peaks were all coincident with lunar semidiurnal tides.

In order to eliminate peaks that were not coincident with the lunar tides, the residuals were histogrammed to tenths of a tidal period to determine which bins contained the greatest numbers of peaks. In this manner those peaks belonging in the most frequented bins were readily identified as lunar semidiurnal tidal peaks, while the remainder were discarded.

A least-squares regression analysis was performed on the final set of residuals to obtain a linear relationship between the residuals and the elapsed number of periods. The slope from this relationship is the estimated rate of clock drift for the meter under consideration. Table 5-1 contains the estimated clock drift for each of the five meters.

Table 5-1. Estimated clock drift

Meter	Days of Operation	Estimated % Drift Rate	Estimated Maximum Time Shift (minutes)
2830	104	0.024	35
2918	57	0.049	40
2919	136	-0.035	-68
2920	141	-0.004	-8
VACM	104*	0.011	17

* Only 104 days were used since this was all that could be matched with Aanderaa No. 2830.

These results show the meters to be within 108 minutes of each other during the 4 month measurement period. This is less than the advertised accuracies (6 minutes per year for the Aanderaa meters and 12 minutes per year for the VACM), but sufficient to perform the type of analyses done for this study.

5.4 CONDUCTIVITY AND SALINITY

The conductivity measurements taken by meter # 2920 were reduced to salinity for the measurement period October 25, 1977 to March 15, 1978. Salinity was calculated by normalizing the conductivity measurements to 15°C and one atmosphere pressure, and then applying the following empirical formula (which is given in the operating manual for the Aanderaa current meters):

$$S = -0.08996 + 28.2972R + 12.80832R^2 - 10.67869R^3 \\ + 5.98624R^4 - 1.32311R^5$$

where S = Salinity in parts per thousand (ppt)

R = The ratio of conductivity of a sample (with a temperature of 15°C and pressure equal to atmosphere) to the conductivity of sample (with a temperature of 15°C, pressure equal to 1 atmosphere, and having a salinity of 35 ppt)

The calculated mean value of salinity for the measurement period was found to be 34.49 ppt. This value is slightly below the historical range (34.6 to 35 ppt) for deep bottom water [5]. The calculated monthly means and ranges are listed below (units = ppt).

<u>Month</u>	<u>Minimum</u>	<u>Mean</u>	<u>Maximum</u>
Oct 1977	34.49	34.59	34.71
Nov 1977	34.23	34.57	34.71
Dec 1977	33.79	34.52	34.64
Jan 1978	33.61	34.49	34.64
Feb 1978	34.29	34.42	34.55
Mar 1978	34.25	34.33	34.53
Full Period	33.61	34.49	34.71

Note: Appendix C contains a histogram of the conductivity measurements from which these salinity statistics were derived.

Appendix H contains summary statistics of the conductivity measurements.

6. DATA INTERPRETATION

Three major pieces of information concerning the Farallon Islands LLW Disposal Site are combined in this section to evaluate the type of currents observed at the site and to derive an estimate for transport potential of waste material from the site. The information used for this evaluation includes the current measurements processed as described in Section 5, the bathymetry describing the depths and slopes in the measurement area, and (see [3]) an evaluation of sediment grain size distributions.

6.1 ANALYSIS OF CURRENTS

Most of the energy stored in deep ocean currents can be characterized by five components listed below.

<u>Current Component</u>	<u>Period</u>	<u>Frequency</u>
Large scale	> 6 months	> 0.0002 cph
Meteorological	3 to 7 days	0.006 to 0.014 cph
Tidal (major)	12 and 24 hrs	0.083 and 0.042 cph
Inertial	12 hr/sin (lat)	Sin (lat)/12 hr
Internal waves	10 min to 8 hr	0.125 to 6.0 cph

Large-scale currents balance pressure gradients resulting from density variations and the Coriolis Force. Since the total measurement time for most current meters is less than 4 months, this current component will appear as part of the mean, or average of the current measurement time series. Meteorological currents result from stress at the sea surface caused by the average wind speed and strength (i.e., length of blow and fetch area) over the ocean. This component will appear as a low frequency part of the current measurement spectrum. Tidal currents result from sea surface displacements caused by astronomical forces. There are approximately 400 different harmonic components of tides that can be classified into three principal components; semidiurnal (12 hours), diurnal (24 hours), and long period (0.5 month, 1 month, 6 months). The semidiurnal tides appear to make up a large part (close to 50 percent) of the total current energy at the Farallon site. Inertial currents may be excited by other currents and propagate because of the coriolis force until they are damped by friction. The period of this component is approximately 20 hours at the latitude of the measurement field. Internal waves and their associated currents are also excited by other currents and propagate along density gradients due to stratification of the ocean. Some energy at internal wave frequencies in the deepwater measurements was observed in the data from meter # 2919 for the months of December and January, as can be seen from examination of the spectra in Appendix E.

The interpretation of the current data from the present study and from previous studies ([6] and [7]) is described below. The data are resolved into periodic components, such as tidal currents, and long-term drift currents. The periodic components are assessed through an examination of the spectral frequency components and the drift currents are assessed by taking long-term vector averages of the current time series. These data products are described in Section 5.1. The relationship between currents measured at the site and large-scale current patterns is also discussed.

6.1.1 Periodic Current Components

The periodic components in the current measurements can be evaluated using the spectrum generated from the measurement time series. The monthly spectra for each meter are given in Appendix E. It can be seen that the measurements are dominated by 12-hour periods corresponding to semidiurnal tides. In general, there is also significant energy in the 20 to 24-hour region, as well as very low frequencies. Occasionally there is also a peak in the spectrum with a 6-hour period in the north-south direction. This situation was most prominent during December 1977 and January 1978 for Aanderaa current meter # 2919. It appears to be the first harmonic of the dominant 12-hour tidal current, and its exact cause is unknown. One possibility is that this peak is due to an internal wave generated by strong tidal currents, which reach their maxima during this period as they flow into and interact with the sloped bathymetry in the area of the trench south of the deployment site.

To examine the major current energy components in more detail, the data was decimated (i.e., resampled with larger sampling intervals) using a finite impulse response digital filter with the following characteristics:

Cutoff frequency: 0.1 cph
 Symmetrical, low pass
 Number of weights: 121
 Cosine taper
 Decimation interval: 3 hours

The spectra for the decimated time series are shown in Figures 6-1 through 6-5. Each spectrum corresponds to the entire measurement record for the respective current meter. The total relative energy, or statistical variance, in the current measurement record can be calculated from:

$$\sum_{i=1}^N S(f_i) \Delta f_i = 1/N \sum_{i=1}^N (X_i^2 - \bar{X}^2)$$

Where X_i = measurement time series
 \bar{X} = mean of series
 N = total number of samples; $i = 1, 2, \dots, N$
 $S(f_i)$ = spectral value at frequency f_i
 Δf_i = frequency resolution (reciprocal of signal length)

The relative energy near various frequencies of interest can be calculated from:

$$E = \sum_{i=j-k}^{j+k} S(f_i) \Delta f_i$$

where 'k' is some number of frequency bins about the frequency bin 'j' of interest; the results are given in Table 6-1. This table shows relative energy (variance) values for low frequencies (less than or equal to 0.01 cycles per hour), 24-hour tides with 20-hour inertial currents, 12-hour tides, and the total mean square energy in the record. It is seen that for the deep near-bottom current meters (# 2918 and # 2919), most of the energy is related to 12-hour tides and is along the east-west axis. However, for the bottom meter # 2920 in the east most section of the measurement area, the current energy (including semidiurnal tides) is slightly greater in the north-south direction. Aanderaa meter # 2830 and the VACM have a more equal energy distribution with a significant low-frequency component dominated by the north-south direction. In conclusion, the periodic tidal energy is dominant in the east-west direction for the deep-site location, and is more multidirectional at the other measurement points. The difference between the total energy and the sum of the current components in Table 6-1 is general noise that is relatively flat through the remainder of the spectrum.

To give an indication of the orientation of the rotary tidal current in the area, tidal ellipses were calculated for the 12-hour energy components listed in Table 6-1. The calculation was performed as described in Figure 6-6, using the cross-spectrum between the north-south and east-west current measurements to compute the phase angle. The results are shown in Figures 6-7 through 6-11. As would be expected, the near-bottom ellipses have a larger ratio of major to minor axes than those for meters in the midwater column (Aanderra # 2830 and the VACM).

The measured current speeds generally range between 0 and 20 cm/s, as can be seen from the time series plots, histograms, and scattergrams given in Appendices A, C, and D, respectively. The speeds exceed 20 cm/s less than 3 percent of the time, and this is discussed in the next section as being relevant to sediment transport.

Table 6-1. Major Current Energy Sources for Entire Operating Period of Each Meter

Meter	Low Frequency to 0.01 cph	Current Components		Total Energy cm/s ²
		Tide (24 hour) Inertial (20 hour)	Tide (12 hour) 0.083 cph	
2918 N-S	--	--	0.5	2.2
2918 E-W	0.4	4.4	14.6	24.2
2919 N-S	--	0.5	0.7	4.6
2919 E-W	0.2	2.9	26.1	35.0
2830 N-S	6.6	2.7	4.3	17.6
2830 E-W	2.5	2.1	5.2	13.0
VACM N-S	9.4	2.4	6.0	22.1
VACM E-W	3.1	2.8	6.9	16.8
2920 N-S	--	0.2	1.4	4.3
2920 E-W	--	0.4	0.8	3.8

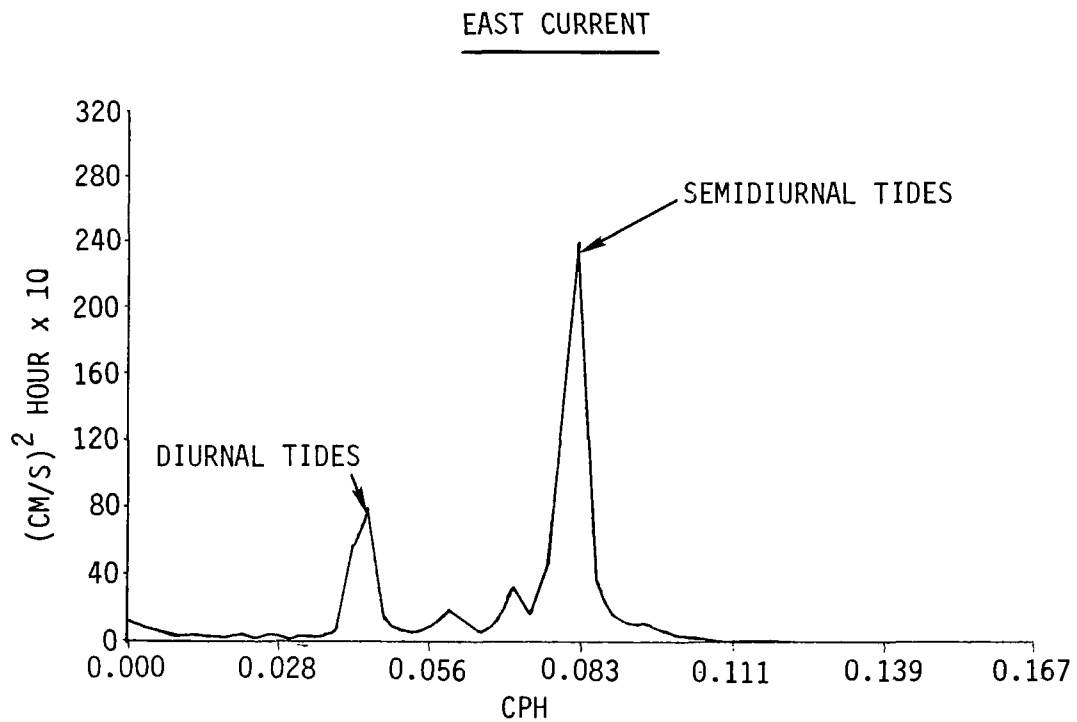
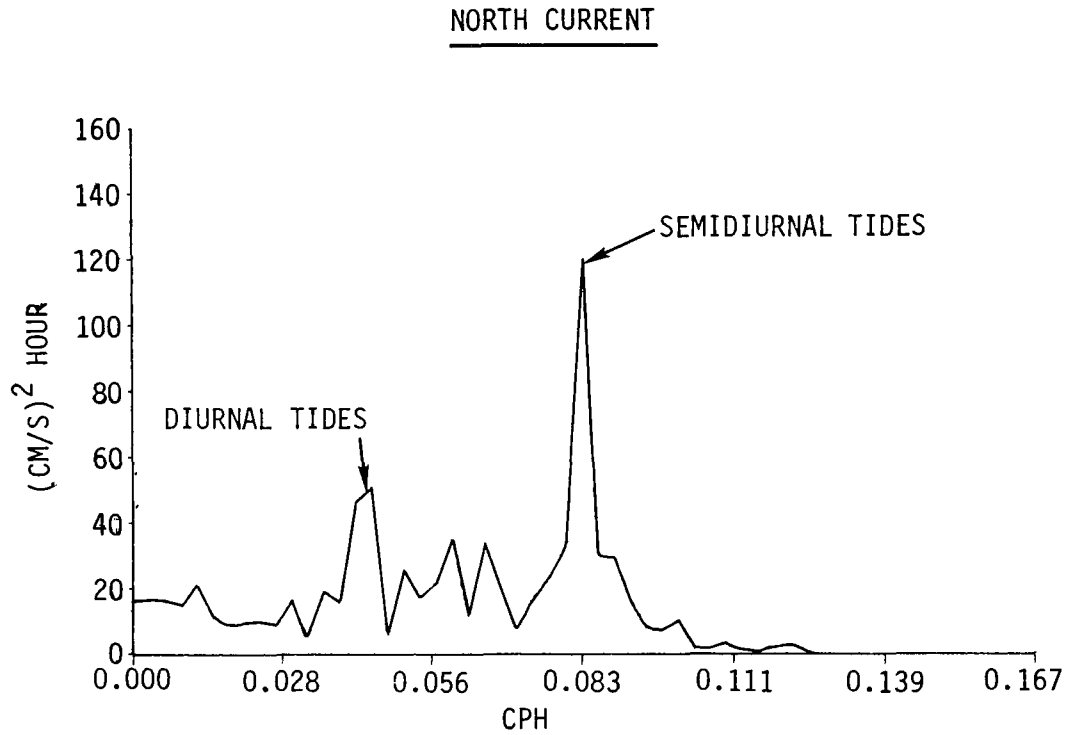


Figure 6-1. Power Spectrum for Meter No. 2918

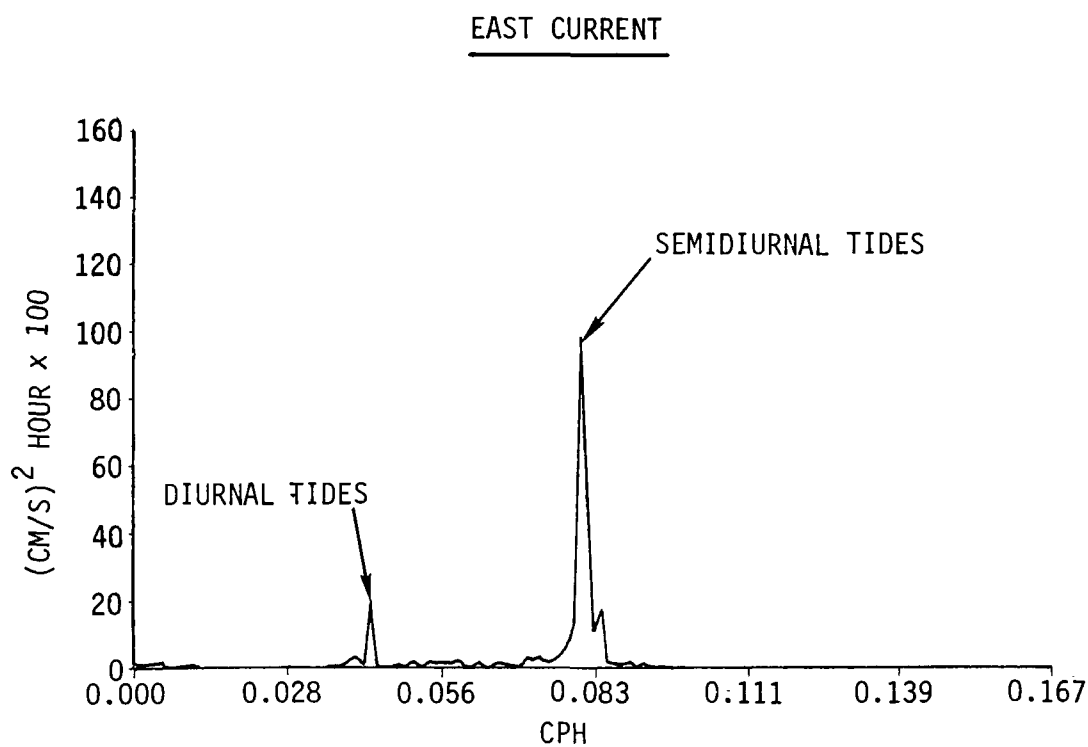
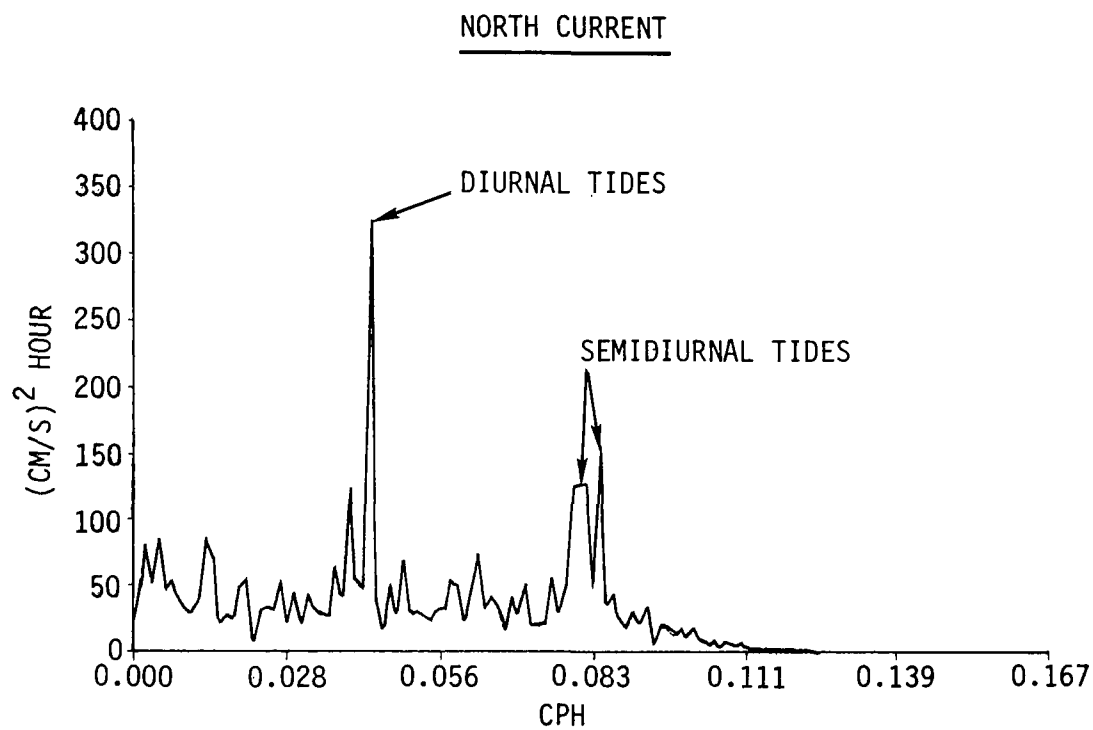


Figure 6-2. Power Spectrum for Meter No. 2919

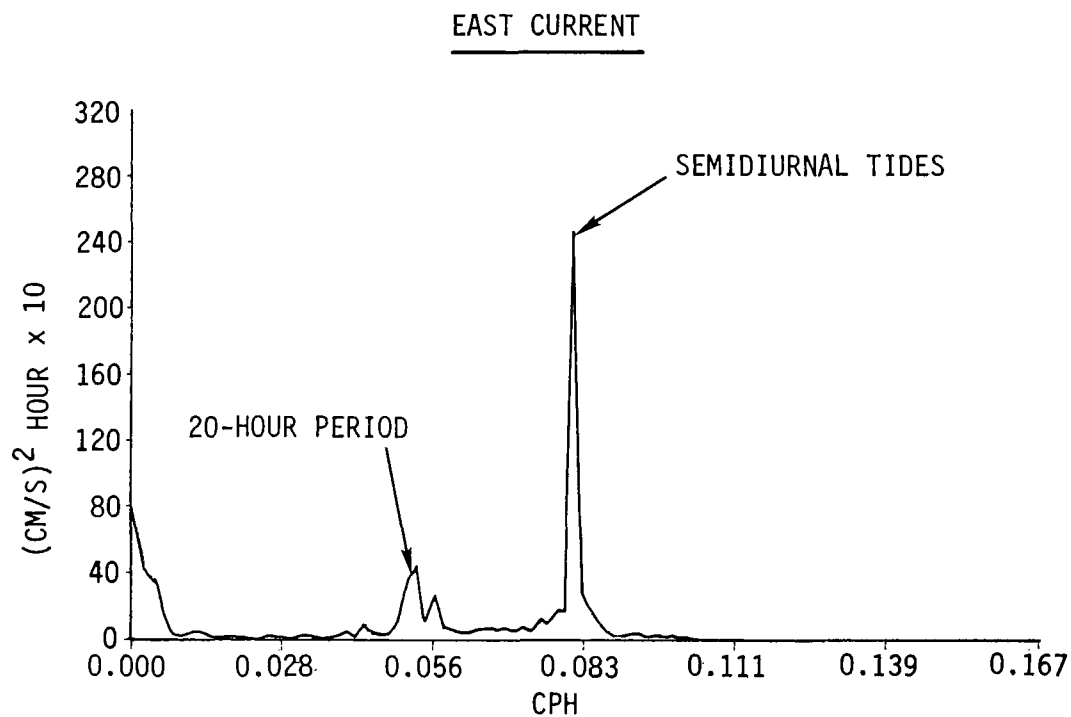
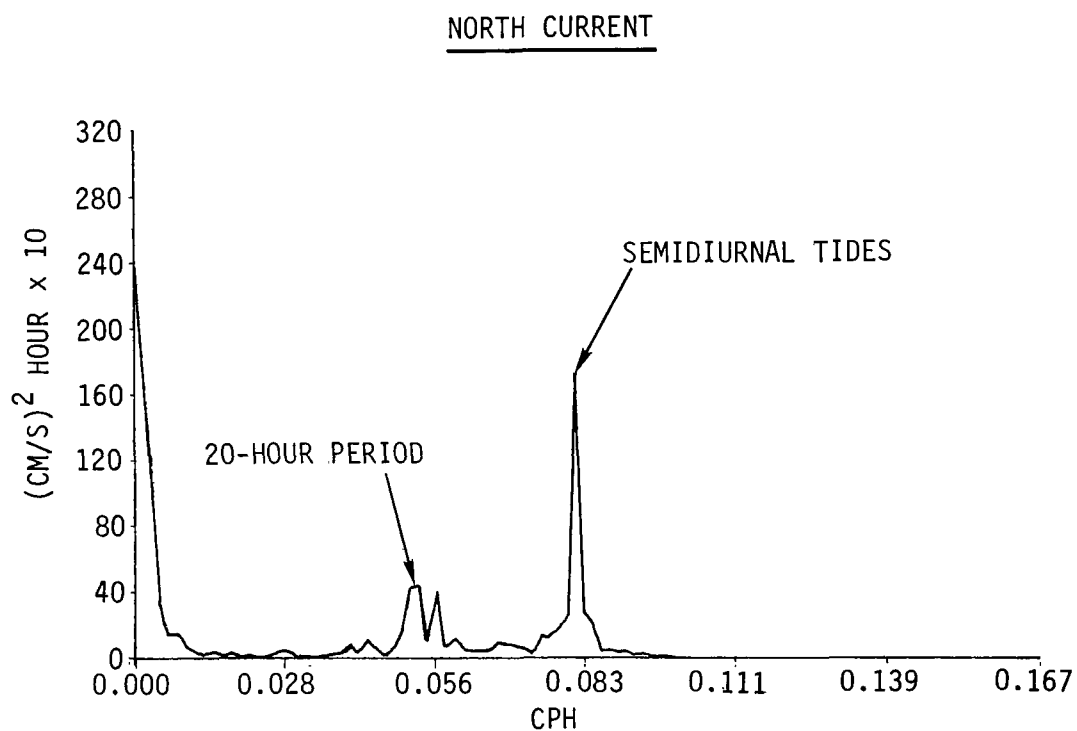


Figure 6-3. Power Spectrum for Meter No. 2830

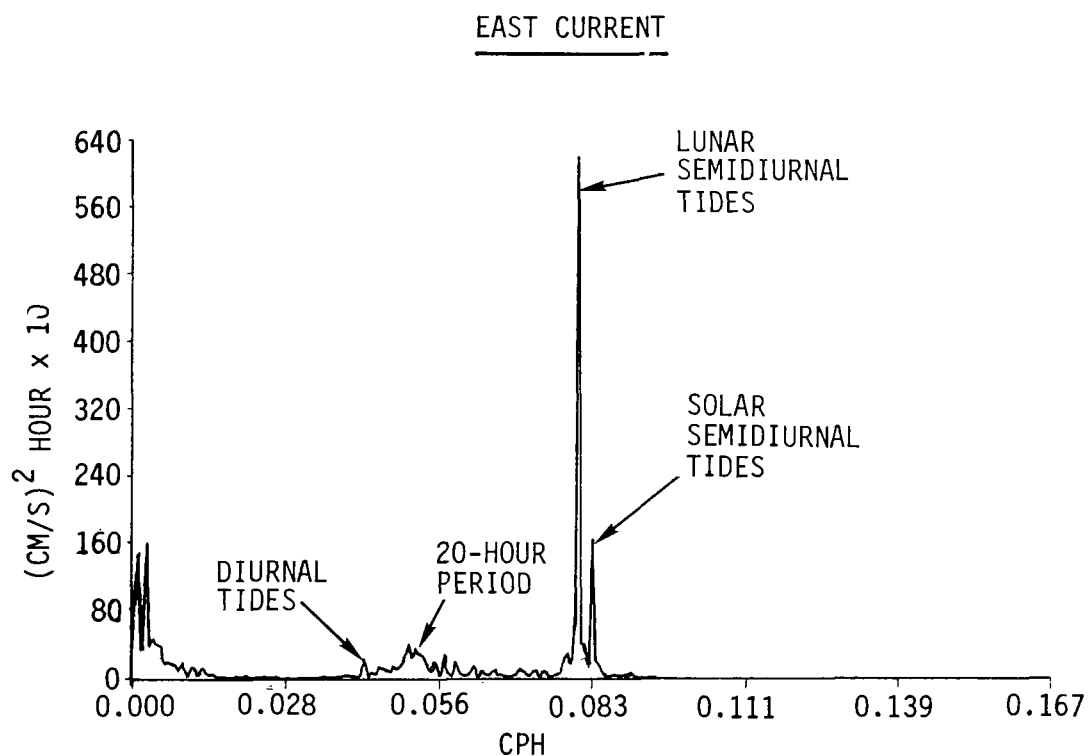
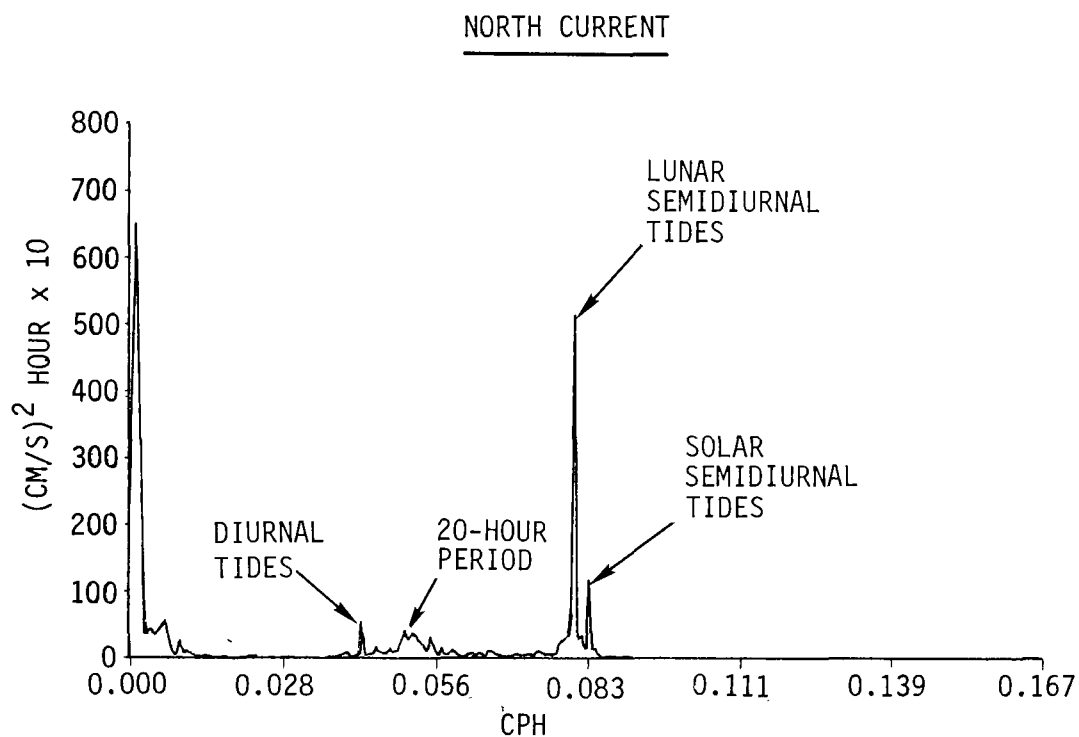


Figure 6-4. Power Spectrum for VACM

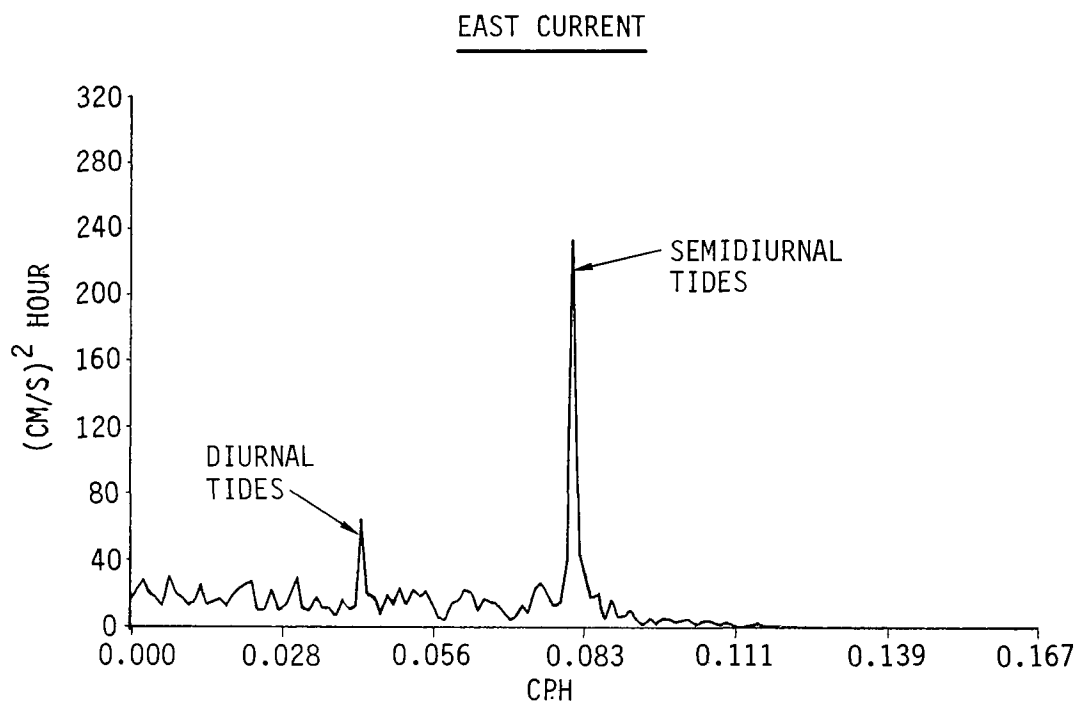
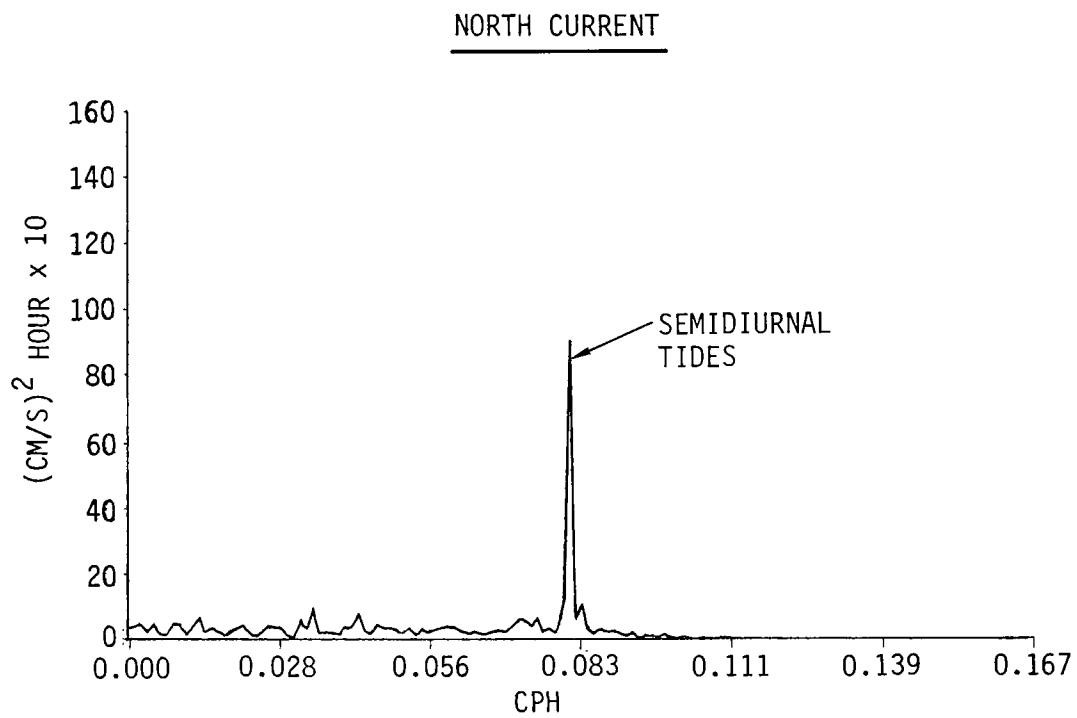


Figure 6-5. Power Spectrum for Meter No. 2920

ROTARY TIDAL CURRENT:

$$\bar{C} = \begin{Bmatrix} C_x \\ C_y \end{Bmatrix}$$

WHERE

$$C_x = A_x \sin (wt + \phi_x) \text{ (east/west)}$$

$$C_y = A_y \sin (wt + \phi_y) \text{ (north/south)}$$

THE VECTOR $\bar{C}(t)$ WILL PARAMETERIZE AN ELLIPSE
BOUNDED BY THE RECTANGLE

$$|C_x| \leq A_x \text{ and } |C_y| \leq A_y$$

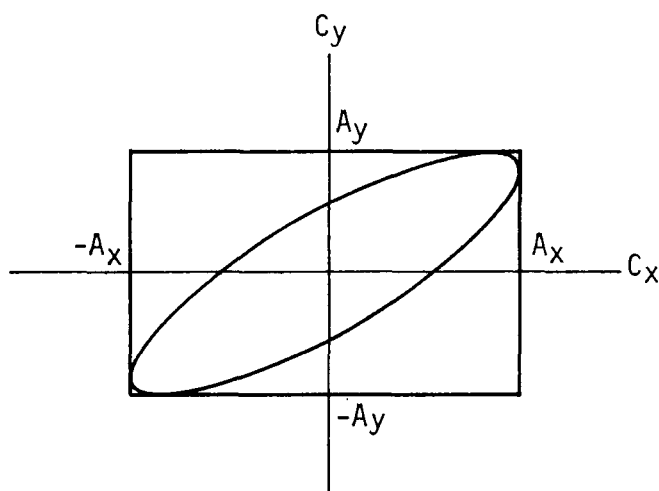


Figure 6-6. Tidal Ellipse Calculation

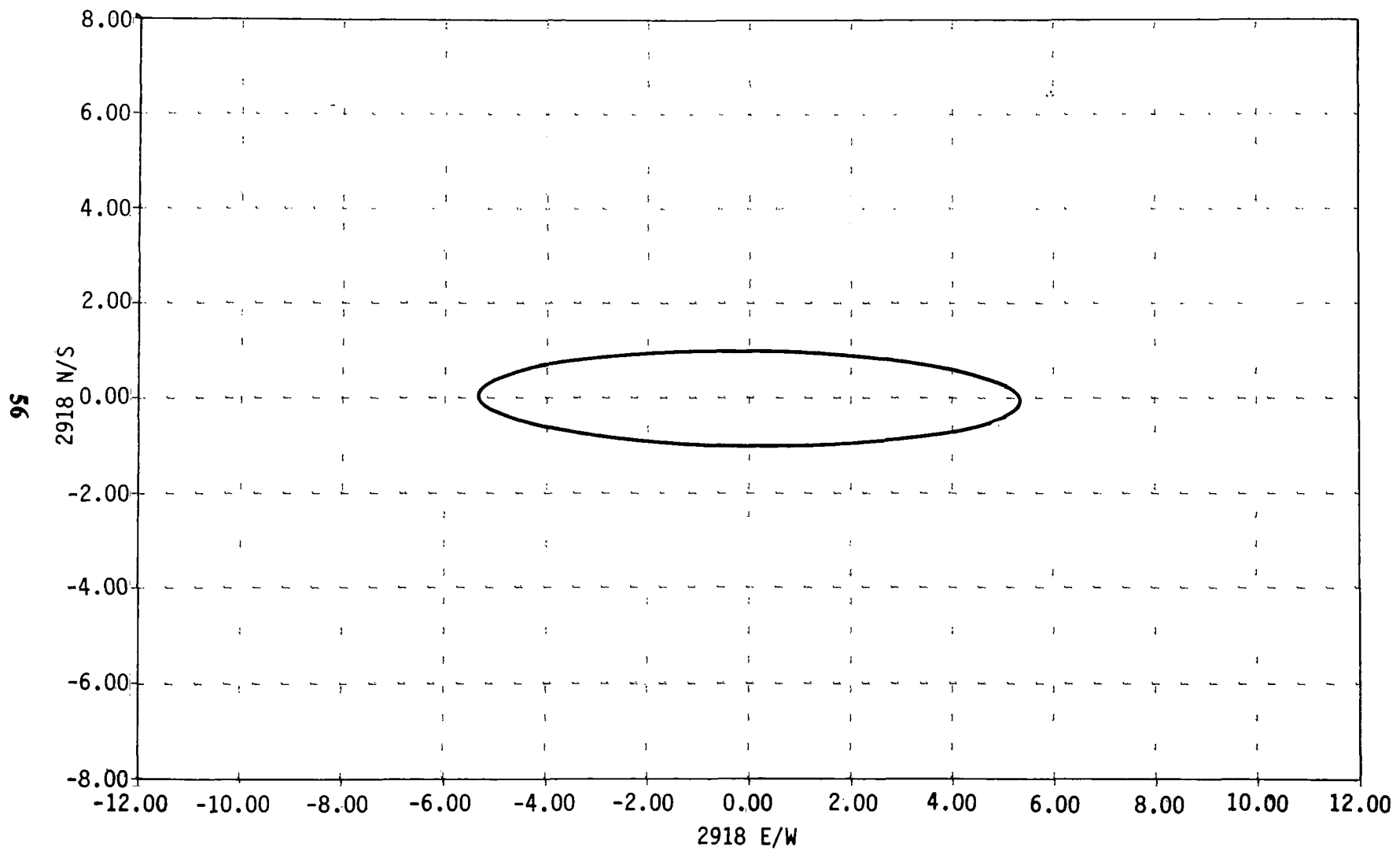


Figure 6-7. Tidal Ellipse for Meter No. 2918

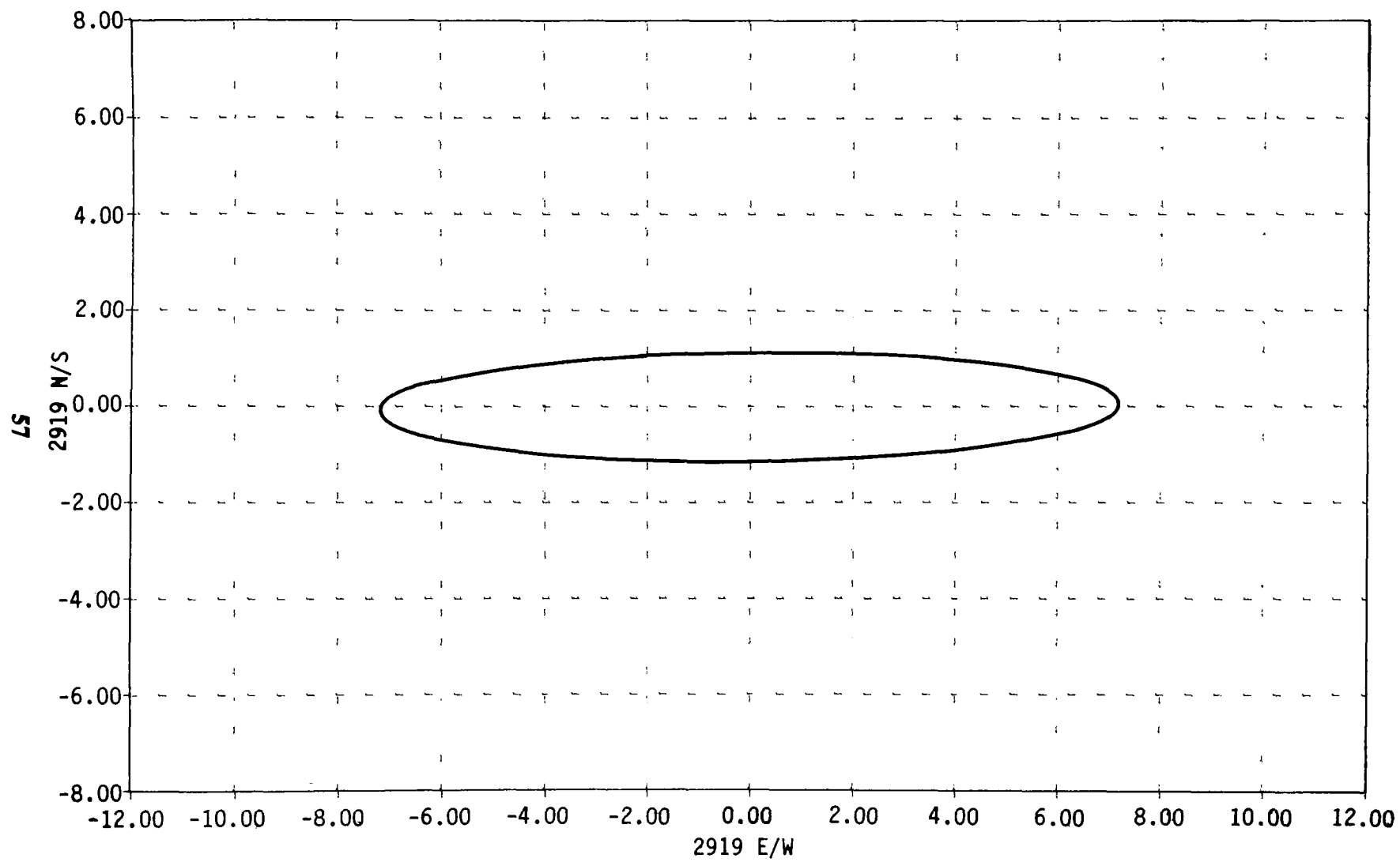


Figure 6-8. Tidal Ellipse for Meter No. 2919

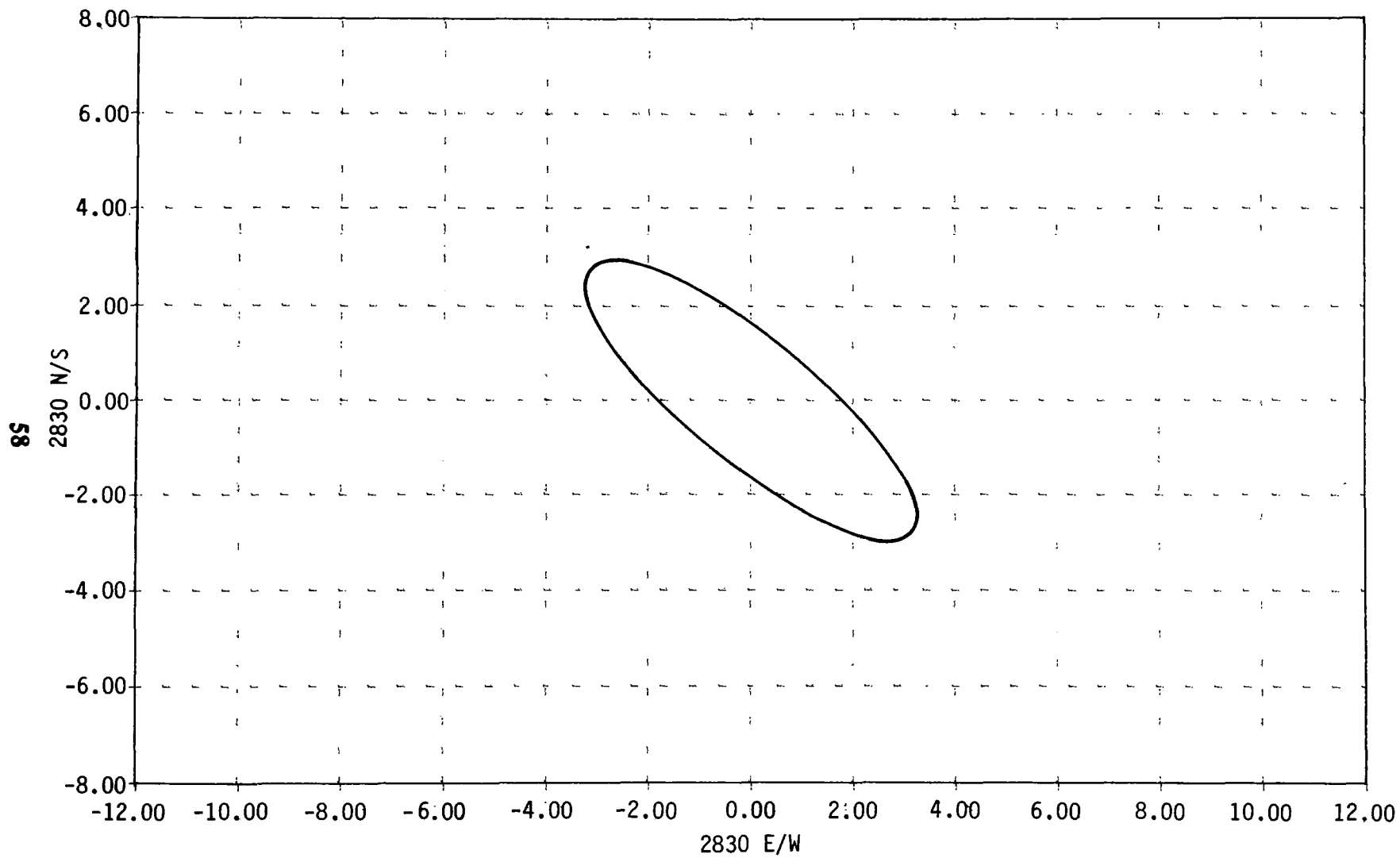


Figure 6-9. Tidal Ellipse for Meter No. 2830

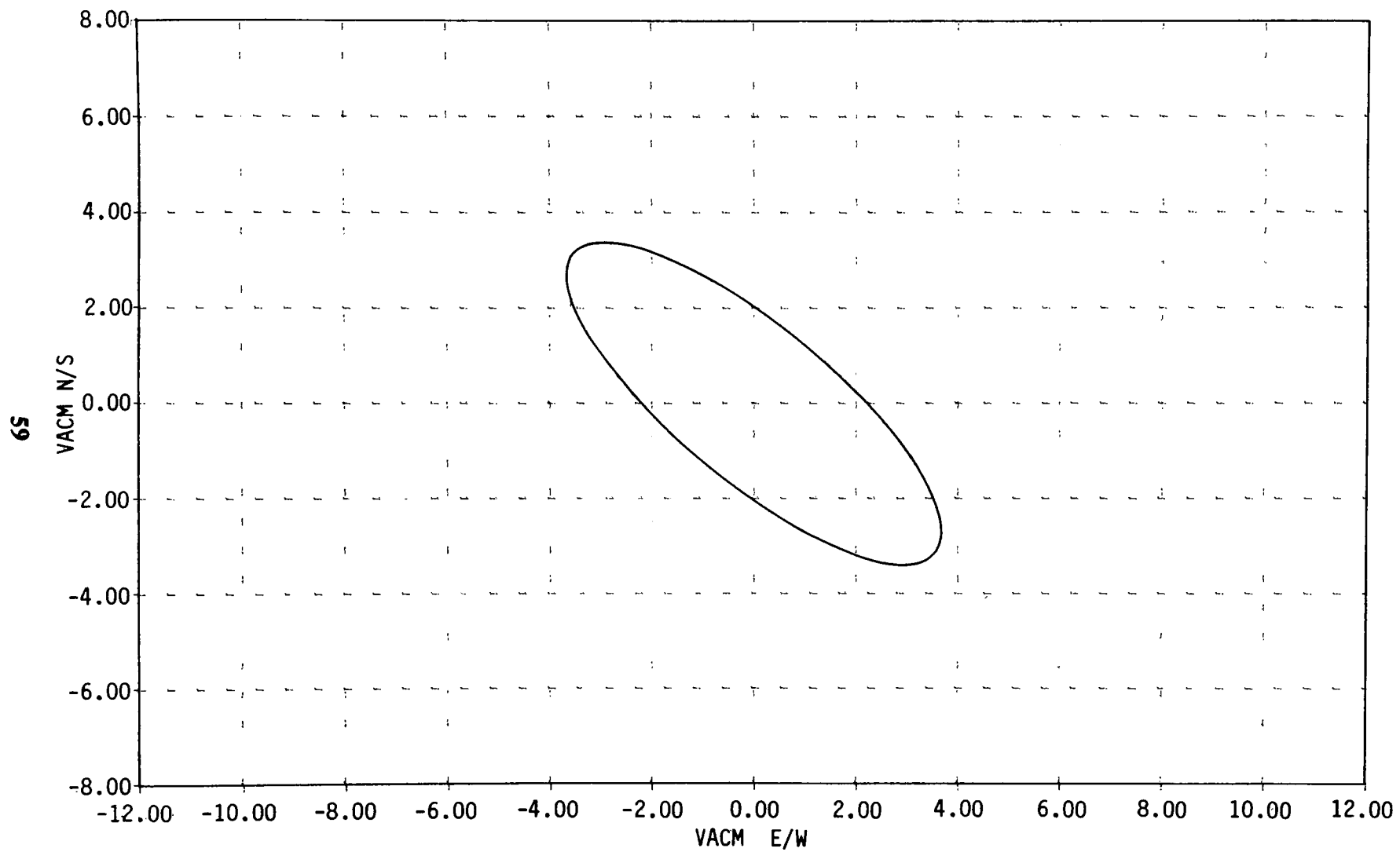


Figure 6-10. Tidal Ellipse for VACM

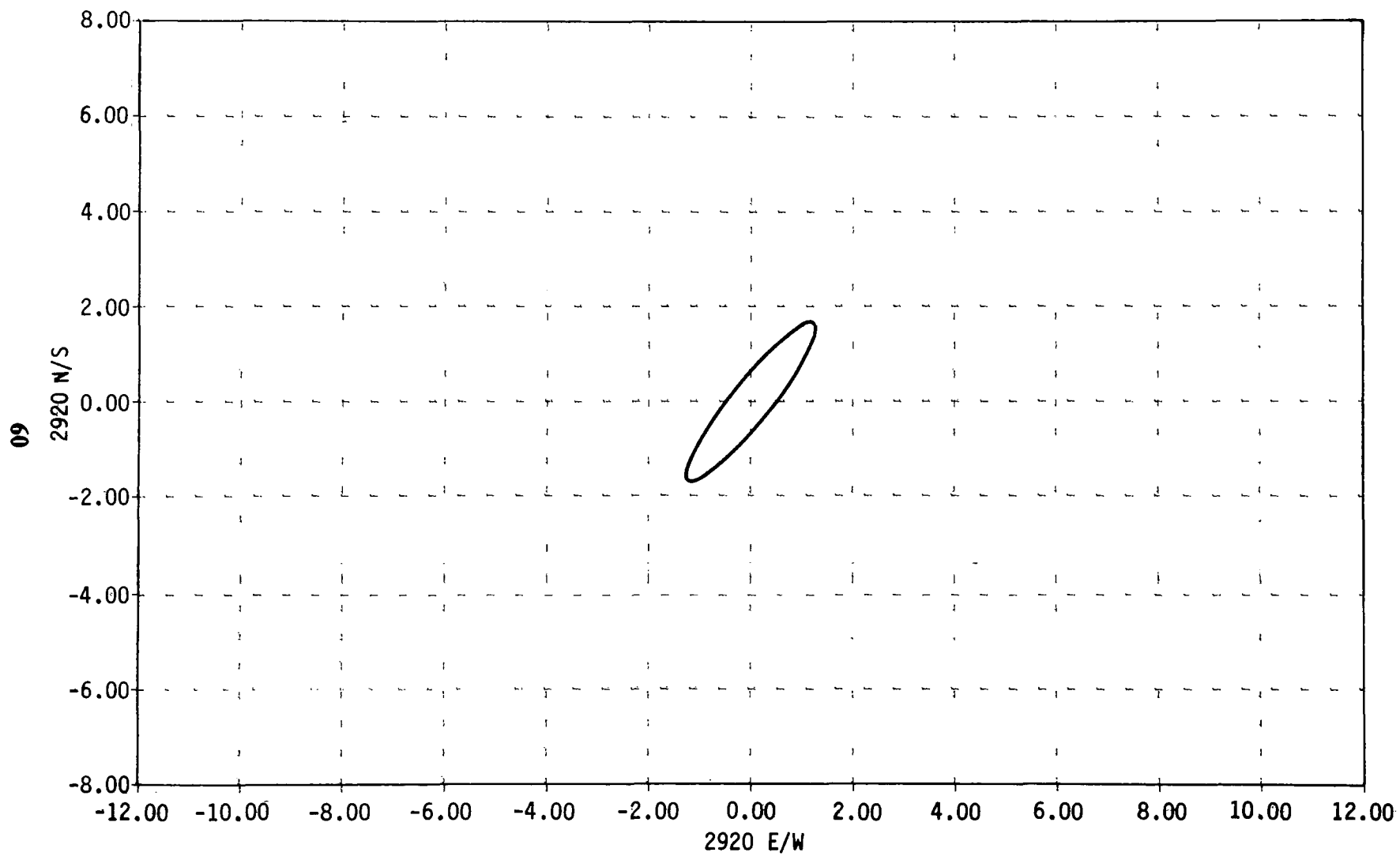


Figure 6-11. Tidal Ellipse for Meter No. 2920

6.1.2 Average Current Components

Long-term average currents were calculated by taking vector averages of the current velocities for each meter. The results are shown in Table 6-2 and depicted graphically by the PVDs given in Appendix F. The average currents are much smaller than the periodic currents (less than 2 cm/s) and move in the northeast quadrant for the bottom measurements and the southeast quadrant for the midwater column measurements.

Table 6-2. Vector-averaged Current Velocities

Meter	Speed (cm/s)	Direction (degrees true)
2918	1.40	69
2919	1.70	2
2830	0.67	137
VACM	0.90	152
2920	0.17	57

In an attempt to determine characteristics of near-bottom circulation patterns within the area, an earlier measurement program (¹⁷¹) deployed two meters above the seafloor near the 1700-meter site in 1975. The current meters, emplaced 21 August 1975 with recordings over a 27-day period, were located 16 kilometers apart and occupied a square centered at 37°38'N and 123°18'W. After removal of the tidal components, bottom currents were found to be clearly north with a mean direction of 004° azimuth and mean velocity of 1.33 cm/s in general agreement with the present (1977-1978) study results.

Although the detailed current structure of the ocean is complex and is not totally understood, there are certain large-scale patterns caused by global forces such as the prevailing winds, tides, and rotation of the earth. These forces produce large-scale patterns in both the surface and deepwater currents that can be seen in the data.

The major surface current off California is the California Current. It moves southward and is part of the north subtropical gyre in the Pacific Ocean, caused by the prevailing winds in the Northern Hemisphere, the continental boundary of North America, and the Coriolis Force. Like all wind-driven currents, it does not penetrate beyond a depth of approximately 100 meters. There is a large-scale deepwater current off California which flows northward, and tends to offset the southward California Current, but it is much slower.

The Coriolis Force (caused by the earth's rotation) tends to give the southward surface current an offshore (westward) component, and the northward deepwater current an onshore (eastward) component. In the coastal region the colder bottom water tends to rise to take the place of the surface water that has been transported offshore.

The general trend of the survey data agrees with this global phenomena, but shows significant variation due to local conditions such as bathymetry. This can be seen from examining the periodic current component energy in Table 6-1 and the long-term average currents in Table 6-2.

6.2 TRANSPORT POTENTIAL

In this section the current data, bathymetry, and sediment grain size are evaluated to determine an estimate of the potential for sediment transport from the waste disposal site. It should be noted that this inquiry makes no claim to present any quantitative estimates of sediment transport paths. However, the data do justify a qualitative assessment of the likelihood that sediments will become suspended, and should this occur, in which general directions transport is most likely. The method followed includes a review of the determined grain size distribution (see [3]); a determination of the potential for suspension of these grain sizes relative to observed current speeds; and, an estimation of transport speed and direction from long-term average currents at each measurement location.

Transport may take place in essentially two modes: (1) transport within the water mass which can be inferred from measurements of two-dimensional observations such as those presented in this report, and (2) bedload transport. To realize transport within the water mass, material must be suspended in that water mass. One important assumption for transport analysis is that suspended material follows water mass motion as a particle of water and without divergence.

Transport at the interface of the water and sediment is called bedload transport. This is a mobilization of the deposited material which moves it horizontally across the bottom, possibly resuspending it for short intervals in a siltation process.

This section considers only the transport of fine-grained sediments (silts and clays) in the water mass for the following reasons:

Grain size analysis (see [3]) shows these relatively fine sediments are present throughout the site region and adjacent areas. In combination they comprise more than half, and usually nearer to 65 percent of the sediment volume (Table 6-3).

The fine-grain sediments offer large surface area-to-volume ratios that enhances the ability to act as a carrier for adsorbed radioactive material.

The site contains packaged waste material. Only when the implosion of the container causes exposure of the surrounding sediments and water to radioactivity is transport of concern.

Coarse material is restricted to transport by major, impulsive events such as slumps or turbidity flows which move short distances with long time periods of no activity in between.

Fine sediment, coupled with currents that exceed 20 cm/s, offer the major possibility for transport over long distances, and at high enough speeds to be seriously considered for impact on regions outside site perimeters. This speed range is approximately the threshold above which sediment resuspension can occur ([5]).

**Table 6-3. Sediment Surface Grain Size Data
from Farallon Islands LLW Site Survey Cores**

Station Number	Sample Depth	Weight Percent			Proportional Sediments (% Fines)
		Sand	Silt	Clay	
13A	0 to 1 cm	28.8	44.8	26.8	71.6%
48	0 to 1 cm	13.8	65.7	20.5	86.2%
47	0 to 1 cm	15.9	61.0	23.1	84.1%
39	0 to 1 cm	38.0	36.5	25.5	62.0%

The data available for this study consist of the observations of currents described in Section 6.1, and grain size distributions (see [3]) from four locations in the area of the dump site extending from water depths of 878 meters to 1350 meters. See [3] for complete descriptions of sampling locations and the analytical techniques applied. It is important to note that a wet-sieve technique was used to determine the distributions at the sample locations.

The arrangement of current meter arrays for the 1977-1978 study was established to describe movement of water at positions near bottom (within 1.5 meters) in an effort to infer where particulate matter would travel while moving near the waste material lying on the bottom. Other meters were suspended at locations in the water column as follows:

A current meter about 30 meters above the bottom at the deepest location to estimate the depth of the boundary layer dynamics and the shift of speed and direction due to boundary layer influences.

Current meters at 911 meters below the surface some 10 kilometers seaward of the near-bottom meter location in 914 meters of water. This approximates a plane permitting examination of the horizontal large-scale motions onshore or offshore from the shallower site.

Because of the nature of the study the conservative assumption is that fine sediments in the form of silts and clays can become suspended in the water mass at current velocities exceeding approximately 20 cm/s. The percent of time that the measured speeds exceeded various velocities was determined for each current meter. The results for 20 cm/s are listed in Table 6-4 and two exceedence diagrams are given in Figures 6-12 and 6-13. Figure 6-12 shows the percent exceedences for all five meters with all of the measurement period considered for each meter. Figure 6-13 shows exceedences with the measurement periods truncated to cover the same period (October through December 1977). The suspension threshold velocity will vary with grain size and cohesivity, but the effect of choosing a different threshold than 20 cm/s can be estimated by referencing these figures.

The following discussion uses a 20 cm/s threshold as its basis. At each near-bottom measurement location, the speeds do become great enough to cause some suspension of the fine-grain sediments. Of the two bottom meters, # 2919 had the greatest percentage of large current speeds, approximately ten times that of meter # 2920. Both meters operated for more than 4.5 months. Since the grain size distribution is similar at both meter locations, it is concluded that a greater potential exists for fine sediment suspension at the western (down slope) end of the site than at the eastern end. The fine-grain sediment will drop out of suspension only at very low current speeds. The speed histograms in Appendix C imply that there will be current velocities sufficient to keep the sediment in suspension for periods of days to weeks once it becomes suspended.

Table 6-4. Percent of Total Time Measurement Speeds Exceed 20 cm/s

Array	Meter	Percent of Time	Total Measurement (Days)
B	2920	0.23	141
C	2830	0.01	104
C	VACM	0.08	365
D	2918	0.77	57
D	2919	2.74	136

For the purposes of this inquiry, transport of fine-grain sediments in suspension can be estimated by examining the long-term vector-averaged velocities given in Table 6-2. At the deep western part of the site, meter # 2919 measured an average speed of 1.7 cm/s (1.46 km/day) due north. Meter # 2918 is 100 meters above # 2919 and gives similar average speeds, predominately in the eastward direction. For sediment in the water column, the general direction of transport is to the northeast (up slope). This can be seen in greater detail from the PVDs in Appendix F. However the average speed measured by # 2920 at the eastern (up slope) end of the site is 0.17 cm/day to the east, which is significantly less than that measured at the western end. Also, # 2830 and the VACM show a southeast movement of 0.67 and 0.90 cm/s, respectively. Since these meters effectively define a horizontal plane with meter # 2920, the onshore transport diminishes significantly at the east end of the site. It therefore appears that there is little chance for any significant transport to continue toward shore; however, there are no explicit measurements to verify this.

In conclusion, current measurements suggest that fine-grain sediment may become suspended with the greatest likelihood of suspension being in deep waters at the western end of the site. Long-term average currents move eastward within the site, but diminish at the shoaling eastern part. The potential for sediment suspension and transport exists, but is small. If necessary, it can be further defined with more detailed analysis, as suggested in Section 7.

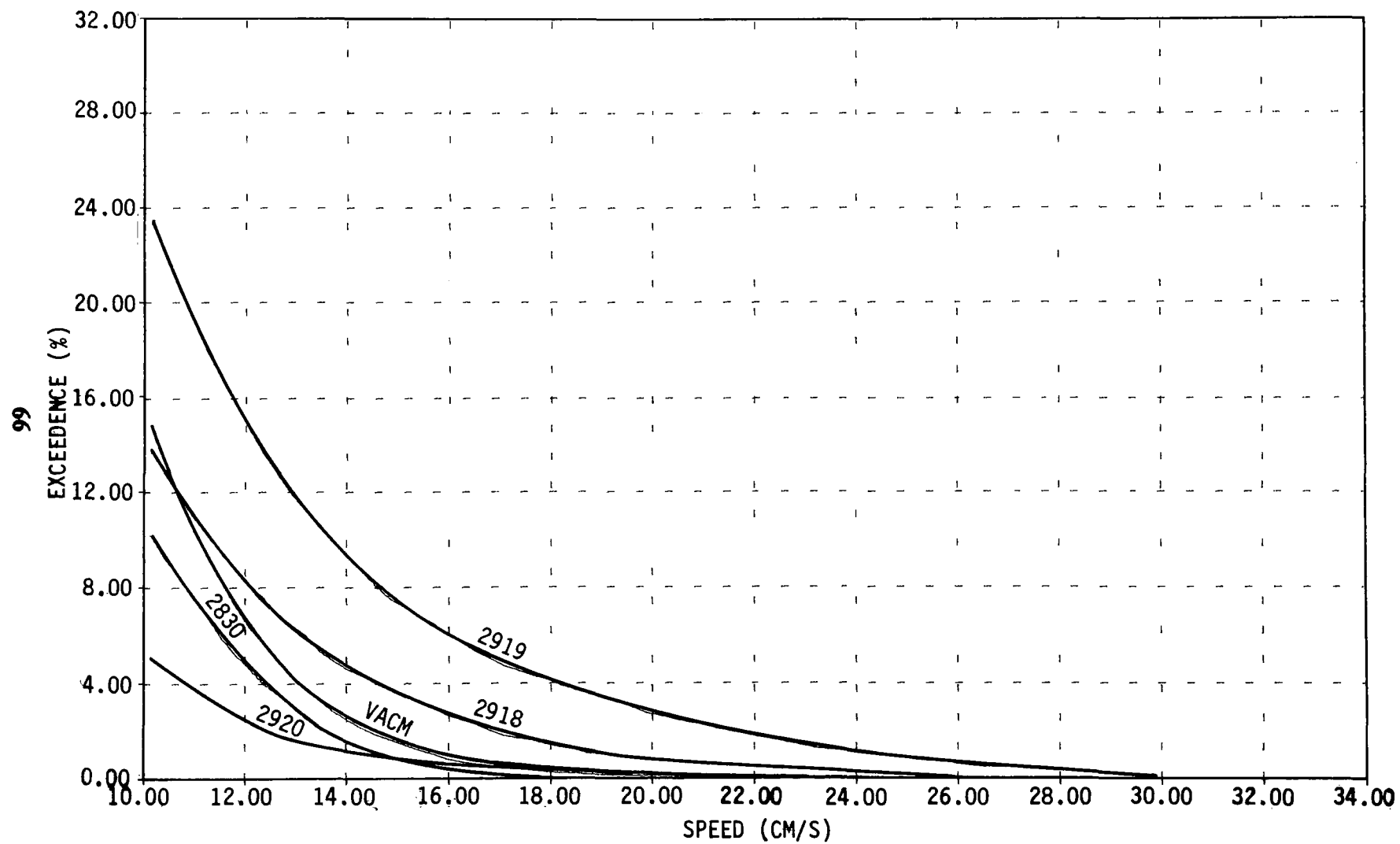


Figure 6-12. Exceedence Curves for Total Measurement Periods

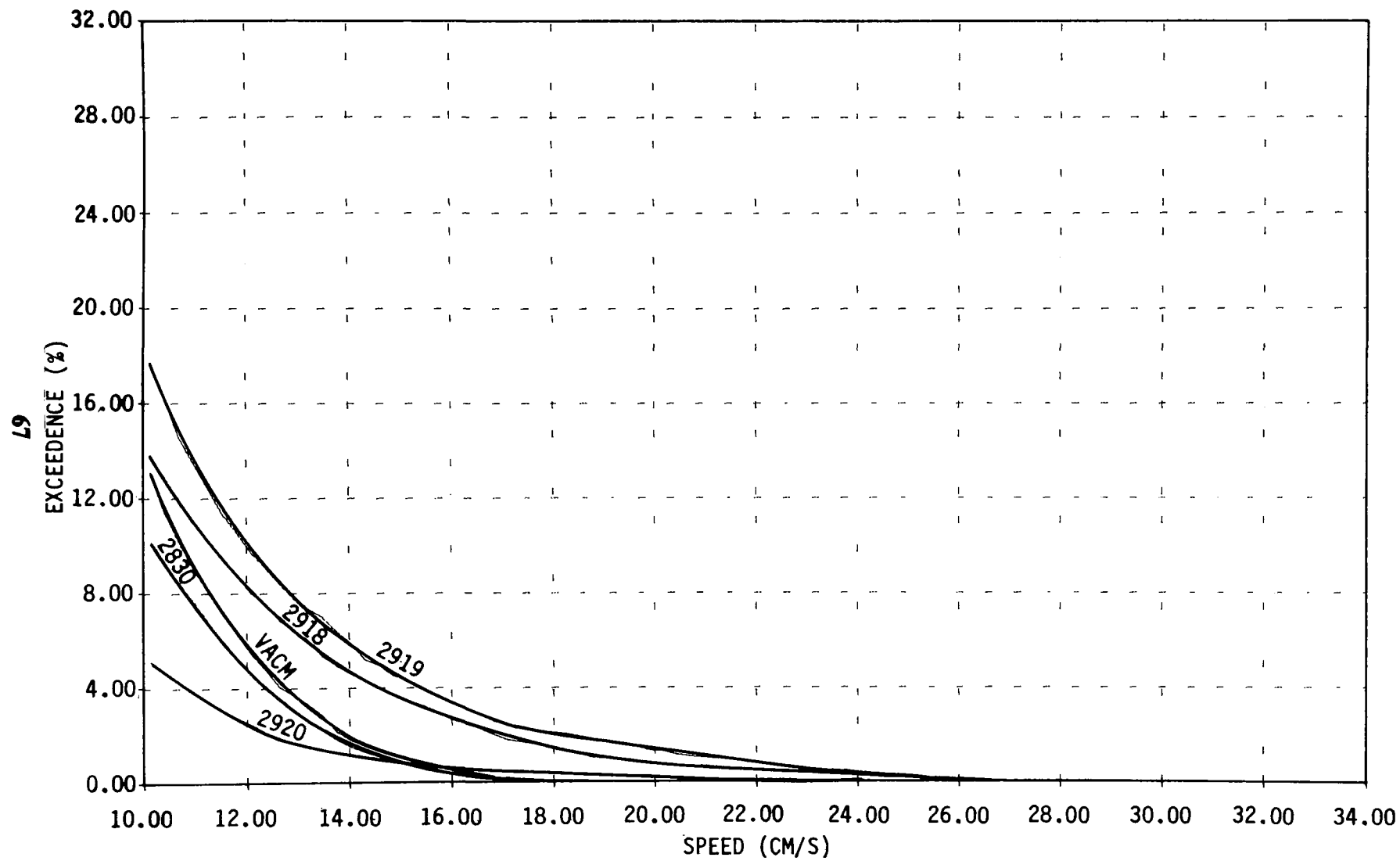


Figure 6-13. Exceedence Curves for October through December 1977

7. RECOMMENDATIONS FOR FURTHER STUDY

A major task for this study was to prepare recommendations for future sampling requirements necessary to develop reliable predictive models for the potential transport of soluble and particulate radioactive materials from formerly used U.S. Pacific Ocean LLW disposal sites. Section 6 described the mechanisms for potential transport based on data accumulated to date. Detailed knowledge of current speeds and sediment composition at the disposal site will yield qualitative information as to whether sediments that may contain radioactive particles from the waste materials could be transported from the site. Transport by ocean currents is believed to be an important mechanism for the possible redistribution of the radioactive materials. The measured speeds from the 1977 survey were great enough so that at least some transport could occur. However, without a more detailed picture of the physical mechanisms involved, the amount and distribution (i.e., direction) of the radioactive sediments cannot be determined.

To develop predictive models which will indicate the probable quantity and direction of the transport of radioactive waste from a disposal site, it is necessary to first develop a conceptual model of the important physical processes involved and their relationships. Presently, there are some gaps in the knowledge of the physics of sediment transport and dispersion of dissolved and suspended particles. However, this should not be a deterrent to the model formulation for various reasons. First, the monitoring and assessment of the potential environmental effects from waste disposal sites is of great concern, and a good conceptual model can be of great use in the design and planning of future measurement programs. The results of the surveys can be used to enhance the model, which will then result in a more effective monitoring program. Second, it may be sufficient to use the model to derive an upper limit for the transport of waste materials. The upper limit can take the extreme case of additive adverse assumptions, and if the resulting exposure is still within acceptable levels, further research of the physical processes becomes less important. If, on the other hand, the results are not within acceptable limits, the model may be further elaborated to see if a more realistic (but more complicated) picture of the physical situation will produce more acceptable results. Thus, in the case of the Farallon Islands study, one may consider the curve for the threshold of sediment transport and suspension as a function of sediment grain size and current speed, to be a very simple conceptual model. If the measured current velocities were not great enough to transport sediment, there would be a strong indication that this is not a problem at the dump site unless the measurements were taken during an unusually calm period. Since this was not the case during this study, it is recommended that further development of a conceptual model be initiated for the distribution and dispersal of radioactive materials from waste disposal sites. This model may take various forms, but is generally a specification of the important physical quantities and boundary conditions with a set of mathematical equations expressing their relationships.

One possible approach would be to consider the current speed and direction data as inputs of a stochastic process, which would generate a set of transport probability distributions based on a well-defined sediment transport formulation such as the Hjulstrom curves ^[81]. This formulation would assign probabilities of initial and sustained suspended transport in terms of current speed and mean grain diameter. Implementing this approach would involve the use of standard Monte Carlo computational procedures. The probabilistic approach could take into account unmeasured or inherently stochastic aspects of the processes being evaluated (i.e., the variability of suspension threshold velocities with the cohesivity of fine grained sediments). It would also offer some direct insight into the degree of uncertainty involved in the predicted transport modes, and statistical confidence units could be ascribed.

To be of the greatest possible utility, the conceptual model (verified and modified by measured data) should be supported by a numerical model. The numerical model is a realization of the conceptual model, which will provide quantitative estimates of the process under investigation for conditions relevant to the area under study. The numerical model can be as simple as a mathematical formula or statistical relationship between the conditions in the area and the resulting effects, or as complex as an evaluation of the coupled equations of motion of all of the important quantities. It is important to also estimate the accuracy of the model to assure that the quality of its predictions are within acceptable limits. It is also important not to make the model more detailed than is justified by the knowledge of the conditions in the area and the physical processes involved. The model can be realized in modular form so that as more information about the area and mechanisms are gathered, it can be easily enhanced to give more accurate predictions. It can then be run under a variety of conditions and assumptions and easily applied to other areas that contain related processes.

A relatively simple procedure for estimating the potential for transport is to implement suspension and bedload transport criteria for a distribution of grain sizes on each of the raw current velocity/direction time series to produce output time series with the following features:

Whenever it is assessed that there is potential for transport (i.e., particle is suspended) the output velocity time series will be set equal to the input time series multiplied by the estimated probability of suspension.

When transport is deemed unlikely (i.e., particle is out of suspension) the output velocity series will be zeroed.

The direction time series is kept identical with the input direction series.

The resulting velocity/direction output series will be a representation of the motion of sediment at the given current meter for each grain size. This time series can then be used to generate PVDs and scattergrams to visually represent the potential for transport as a function of direction. The sensitivity of these estimates (and hence the amount of uncertainty) will be largely reflected in the amount of variation of the PVDs as a function of grain size.

The most direct and accurate determinations of the physical conditions in an area of the ocean are determined from direct measurements. Measurement programs are, however, expensive, and therefore limited in both spatial extent and temporal coverage. It is usually essential that any oceanographic investigation be supported by some measured data, as was provided by the present Farallon Islands LLW disposal site study. It is desirable that the program be designed with a conceptual model of the important processes taken into account, and that the results be used to test, verify, and calibrate the model.

It is believed that additional current measurements would yield a greater understanding of the potential for transport of radioactive materials in the case of the Farallon Islands LLW disposal site. Measurements of deepwater currents are rare and difficult to obtain, and the success of the survey analyzed in this report is encouraging. However, only one of the meters was capable of recording data for an entire year. The others recorded data for the late fall and winter seasons only. In addition, it is not known whether the data was taken during a typical year, or a year with unusually low or high activity. Additional data would help to answer this question and provide a greatly increased statistical data base from which assessments of conditions in the area can be made. Statistical data for normal and extreme conditions are of importance. Once both of these data bases have been collected and are large enough to inspire confidence, the area can be characterized in a statistical sense, and projections of current related processes can be derived for the future.

If more current measurements are to be obtained, it is recommended that a careful calibration program on all instruments be carried out. The present study provided an excellent opportunity to compare the responses of two commonly used current meters: the Aanderaa and VACM. These gave the same general statistical results, but differed somewhat in their detailed time series measurements under the same conditions.

8. REFERENCES

- [1] Joseph, A. 1957. United States' Sea Disposal Operations, A Summary to December 1956. Technical Information Service Report No. WASH-73. United States Atomic Energy Commission, Washington, DC.**
- [2] Noshkin, V. E. 1978. Radionuclides in the Marine Environment near the Farallon Islands. Lawrence Livermore Laboratory, Univ. of California, Livermore.**
- [3] Dayal, R., Duedall, I.W., Fuhrmann, M. and Heaton, M.G. 1979. Sediment and Water Column Properties at the Farallon Islands Radioactive Waste Dumpsites. Final report to the Office of Radiation Programs. U. S. Environmental Protection Agency, Washington, DC.**
- [4] Wilde, P. 1976. Oceanographic Data Off Central California, 37° to 40° North Including the Delgada Deep Sea Fan. LBL Pub. 92. Lawrence Berkeley Laboratory, Univ. of California, Berkeley.**
- [5] Sverdrup, H., Johnson, M.U. and Fleming, R.H. 1955. The Oceans - Their Physics, Chemistry and General Biology. 6th ed. Prentice-Hall, Inc. Englewood Cliffs, NJ.**
- [6] U.S. Environmental Protection Agency. 1983. Analysis of Ocean Current Meter Records Obtained from a 1975 Deployment off the Farallon Islands, California. Office of Radiation Programs, Washington, DC. EPA 520/1-83-019.**
- [7] Dyer, R. 1976. Environmental Surveys of Two Deep Sea Radioactive Waste Disposal Sites Using Submersibles. Proceedings of an International Symposium on Management of Radioactive Wastes From the Nuclear Fuel Cycle, Vol. I. International Atomic Energy Agency, Vienna, Austria. Pages 317-338. IAEA-SM-207/65.**
- [8] Hjulstrom, R. 1935. Studies of the Morphological Activity of Rivers as Illustrated by the River Fyris. Bull. of the Geol. Inst., Uppsala, Sweden. Vol. 25, Pages 221-527.**

9. BIBLIOGRAPHY

Aanderaa Instruments. 1976. Operating Manual for Recording Current Meter Model 5. Aanderaa Instruments, Bergen, Norway.

AMF Sea-Link Systems. 1976. Vector Averaging Current Meter. AMF Sea-Link Systems, Herndon, VA.

Bendat, J.S. and Piersol, A.G. 1971. Random Data: Analysis and Measurement Procedures. Wiley-Interscience, NY.

Bouma, A.H. 1962. Sedimentology of Some Flyash Deposits, Elsevier, Amsterdam, Netherlands.

Carney, R. S. 1979. A Report on the Invertebrate Megafauna Collected by Otter Trawl at the Farallon Islands Radioactive Waste Disposal Site during the August, September and October, 1977 Cruises of the R/V Velero. Prepared for the Office of Radiation Programs. U.S. Environmental Protection Agency, Washington, DC.

Conomos, T.J., McCulloch, D.S, Peterson, D.H., and Carlson P.R. 1971. Drift of Surface and Near Bottom Waters of the San Francisco Bay System, March 1970-April 1971. Miscellaneous Field Studies Map, M.F. 333. U.S. Geological Survey, Reston, Virginia.

Dayal R., Oakley, S. and Duedall, I.W. 1976. Sediment-Geothermal Studies of the 2800 m Nuclear Waste Disposal Site. Final report to the Office of Radiation Programs, U.S. Environmental Protection Agency, Washington, DC.

Defant, A. 1961. Physical Oceanography Vols. I & II. MacMillan Co., NY.

Friedman, G.M. and Sanders, J.E. 1978. Principles of Sedimentology. John Wiley & Sons, NY.

Goldberg, E.D. et al., eds. 1977. The Sea: Ideas and Observations on Progress in the Study of the Seas. Vol. 6: Mar. Modeling. John Wiley and Sons, NY.

Gotshall, D.W. and Dyer, R.S. 1987. Deepwater Demersal Fishes Observed From The Submersible AVALON (DSRV-2) Off The Farallon Islands, 24 June 1985. Marine Resources Technical Report # 55. California Department of Fish and Game, Long Beach, California.

BIBLIOGRAPHY (continued)

Hill, M.N., ed. 1962. The Seas: Ideas and Observations on Progress in the Study of the Seas. Vol. 1: Phys. Oceanog. John Wiley and Sons, NY.

Keenan, Pat. 1980. Aanderaa RCM Compass Errors. Exposure; a Newsletter for Ocean Technologists. Vol. 8, No. 2.

Kuenen, P.H. 1953. Significant Features of Graded Bedding. Bull. of American Assoc. of Petrol. Geol. Vol. 37., Pages 1044-1066.

Reish, D.J. 1978. Study of the Benthic Invertebrates Collected from the United States Radioactive Waste Disposal Site off the Farallon Islands, California. Prepared for the Office of Radiation Programs. U. S. Environmental Protection Agency, Washington, DC.

Schell, W.R. and Sugai, S. 1978. Radionuclides in Water, Sediment and Biological Samples Collected in August-October, 1977 at the Radioactive Waste Disposal Site Near the Farallon Islands. Final report to the Office of Radiation Programs, U.S. Environmental Protection Agency, Washington, DC.

Shepard, F. P. 1973. Submarine Geology. 3rd ed. Harper & Row Pub., NY.

Swift, D.J. et al., eds. 1973. Shelf Sediment Transport: Process & Pattern. Academic Press, Inc., NY.

U.S. Environmental Protection Agency. 1975. A Survey of the Farallon Islands 500 Fathom Radioactive Waste Disposal Site. Office of Radiation Programs, Washington, DC. Tech Note ORP 75-1.

U.S. Environmental Protection Agency. 1982. Analysis of Current Meter Records at the Northwest Atlantic 2800 meter Radioactive Waste Dumpsite. Office of Radiation Programs, Washington, DC. EPA 520/1-82-002.

U.S. Environmental Protection Agency. 1983. Survey of the Marine Benthic Infauna Collected from the United States Radioactive Waste Disposal Sites off the Farallon Islands, California. Office of Radiation Programs, Washington, DC. EPA 520/1-83-006.

U.S. Environmental Protection Agency. 1988. A Study of Deep-Ocean Currents Near the 3800 m Low-Level Radioactive Waste Disposal Site, May 1984 - May 1986. Office of Radiation Programs, Washington, DC. EPA 520/1-88-007.

BIBLIOGRAPHY (continued)

U.S. Environmental Protection Agency. 1988. Waste Package Performance Criteria for Deepsea Disposal of Low-Level Radioactive Waste. Office of Radiation Programs, Washington, DC. EPA 520/1-88-009.

U.S. Environmental Protection Agency. 1988. A Monitoring Program for Radionuclides in Marketplace Seafoods. Office of Radiation Programs, Washington, DC. EPA 520/1-88-010.

U.S. Environmental Protection Agency. 1988. Sediment Monitoring Parameters and Rationale for Characterizing Deep-Ocean Low-Level Radioactive Waste Disposal Sites. Office of Radiation Programs, Washington, DC. EPA 520/1-87-011.

U.S. Environmental Protection Agency. 1989. A Review and Evaluation of Principles Used in the Estimation of Radiation Doses Associated with Deep-sea Disposal of Low-Level Radioactive Waste. Office of Radiation Programs, Washington, DC. EPA 520/1-89-019.

U.S. Environmental Protection Agency. 1990. Analysis and Evaluation of a Radioactive Waste Package Retrieved from the Farallon Islands 900-meter Disposal Site. Office of Radiation Programs, Washington, DC. EPA 520/1-90-014.

U.S. Environmental Protection Agency. 1990. Recovery of Low-Level Radioactive Waste Packages from Deep-Ocean Disposal Sites. Office of Radiation Programs, Washington, DC. EPA 520/1-90-027.

TECHNICAL REPORT DATA
(Please read Instructions on the reverse before completing)

1. REPORT NO. EPA 520/1-91-009		2.	3. RECIPIENT'S ACCESSION NO.	
4. TITLE AND SUBTITLE Ocean Current Measurements at the Farallon Islands Low-Level Radioactive Waste Disposal Site, 1977-1978			5. REPORT DATE April 1991	
			6. PERFORMING ORGANIZATION CODE	
7. AUTHOR(S) D. Crabbs, R. Crane, and D. Friedlander			8. PERFORMING ORGANIZATION REPORT NO.	
9. PERFORMING ORGANIZATION NAME AND ADDRESS Interstate Electronics Corporation 1001 East Ball Road Anaheim, CA 92803			10. PROGRAM ELEMENT NO.	
			11. CONTRACT/GRANT NO. Contract 68-01-0796	
12. SPONSORING AGENCY NAME AND ADDRESS U.S. Environmental Protection Agency Office of Radiation Programs (ANR-461) 401 M Street, SW Washington, DC 20460			13. TYPE OF REPORT AND PERIOD COVERED Final	
			14. SPONSORING AGENCY CODE ANR-461	
15. SUPPLEMENTARY NOTES				
16. ABSTRACT This report presents data from an ocean current measurement study, conducted during 1977 and 1978, in the area of the Farallon Islands low-level radioactive waste (LLW) disposal site off the coast of San Francisco, California. The purpose of this study was to measure near-bottom and bottom currents in the area, and utilize available historical data, to determine the potential for transport of LLW from the disposal site toward populated areas in the vicinity of San Francisco. Interpretation of the current meter data combined with other available data taken at the site during previous studies in 1974 and 1975 is also presented. The appendices to the report contain computer generated graphical displays of the output data from all the current meters.				
17. KEY WORDS AND DOCUMENT ANALYSIS				
a. DESCRIPTORS		b. IDENTIFIERS/OPEN ENDED TERMS		c. COSATI Field/Group
1. ocean disposal 2. low-level radioactive waste disposal 3. radionuclide transport 4. ocean bottom currents				
18. DISTRIBUTION STATEMENT Release Unlimited		19. SECURITY CLASS (This Report) Unclassified		21. NO. OF PAGES 84
		20. SECURITY CLASS (This page) Unclassified		22. PRICE